# Impact of stylolites on the mechanical strength of limestone

Patrick Baud, Alexandra Rolland, Michael Heap, Tao Xu, Marion Nicolé, Thomas Ferrand, Thierry Reuschle, Renaud Toussaint, Nathalie Conil

# Impact of stylolites of the mechanical strength of limestone

**Patrick Baud[1], Alexandra Rolland[1], Michael Heap[1], Tao Xu[2], Marion Nicolé[1], Thomas Ferrand[3], Thierry Reuschlé[1], Renaud Toussaint[1], Nathalie Conil[4]**

*[1]Institut de Physique du Globe de Strasbourg (UMR 7516 CNRS, Université de Strasbourg/EOST), 5 rue René Descartes F-67084 Strasbourg Cedex, France.*

*[2]College of resources and Civil Engineering, Northeastern University, Shenyang, China*

*[3]Département de Géologie, Ecole Normale Supérieure, Paris, France*

*[4]ANDRA, Bure, France*

* *Corresponding author*

## ABSTRACT

We performed series of uniaxial compression tests on samples of microporous carbonates from the formations surrounding the ANDRA Underground Research Laboratory in Bure, France. Sedimentary stylolites are pervasive in these formations. We show that the porosity in the vicinity of the stylolites is always larger than that of the host rocks. As a result, our new mechanical data reveal that samples with a stylolite are always significantly weaker with respect to the adjacent stylolite-free material. However the presence of a stylolite in different orientations (with respect to the direction of loading) did not result in any mechanical anisotropy. Numerical simulations using a 2D finite element code suggest that the weakening induced by the presence of a stylolite is mostly due to the higher porosity and the higher level of heterogeneity in and around the stylolite, while the absence of mechanical anisotropy is due to the roughness of the stylolite. While the presence of stylolites weakens carbonate rocks, stylolites only act as planes of weakness when their thickness exceeds a certain threshold (about 5 mm).

## 1. Introduction

Stylolites are the product of intergranular pressures-solution and are pervasive in sedimentary formations. They have been described in carbonates (Stockdale, 1943; Park and Schot, 1968; Bathurst, 1971), sandstones (Heald, 1955; Baron and Parnell, 2007), and shales (Rutter, 1983). They appear as column-and-socket interdigitation features (Nenna and Aydin, 2011; Croizé et al., 2013) and are filled with insoluble elements such as organic matter, oxides, or clay particles (Nelson, 1983). Stylolites grow orthogonal to the major principal stress and are often divided in two groups: sedimentary stylolites oriented sub-horizontally to bedding (i.e., those that form due to overburden stresses) and tectonic stylolites (perpendicular or oblique to bedding).

Stylolites have interested geoscientists for now almost a century primarily because, as compaction localization features, they could potentially impact fluid flow at various scales. Until recently, prevalent views on this matter were that stylolites were barriers to fluid flow (see for example Dunnington, 1967). Recent experimental studies revealed however that stylolites in limestones do not influence permeability when they are oriented perpendicular to fluid flow but could in some cases act as conduits when orientated parallel to flow (Lind et al., 1994; Heap et al. 2014a; Rustichelli et al., 2015). In the last decade, several studies also attempted to use stylolites as palaeostress gauges by linking their morphology to *in situ* stresses (e.g., Schmittbuhl et al., 2004; Rolland et al., 2012).

In situations where stylolites are abundant, another outstanding question important for reservoir/aquifer production and a wide variety of geotechnical applications is their impact on the mechanical strength and rheology of sedimentary formations. This question raised less attention from the scientific community perhaps because its answer appeared somehow obvious. The prevalent views are that the presence of stylolites significantly weakens rocks (Yates and Chakrabarti, 1998; Larbi, 2003; Özvan et al., 2011), that stylolites are natural

planes of weakness in sedimentary formations (Nicholson and Nicholson, 2000; Pires et al., 2010), and that they induce a significant mechanical anisotropy (Rashed and Sediek, 1997). The fact that stylolites weaken a rock mass is supported by many observations in quarries. López-Buendía et al. (2013), for example, noted that more than 95% of the breakages affecting the Crema Marfil marble at thin dimensions in a quarry were due to stylolites. Although very low strength was reported in Brazilian tests on the same material with open stylolites (López-Buendía et al., 2013), no study has, to our knowledge, systematically quantified the impact of stylolites on rock strength. One reason is probably that, in both field and laboratory contexts, the opening of the stylolites due to drilling, cutting, or depressurization, is a major issue and there is always some ambiguity whether the observed effect could in fact not primarily be due to some significant microcracking/fracturing associated to the stylolites and not to the structure itself. To what extent are stylolites planes of weakness if they are not open? Do they induce any mechanical anisotropy in that case, and is it possible to systematically quantify some related weakening, if it exists at all? To answer these questions we performed series of uniaxial compression tests on samples prepared from cores taken from a borehole drilled in a limestone formation in the Paris Basin. Stylolites are abundant in this formation and Heap et al. (2014a) recently showed that it is possible to prepare samples in various orientations without opening the stylolites. We are therefore able to systematically compare the mechanical behavior of these limestones with and without stylolites. Guided by new petrophysical measurements and microstructural observations, numerical modelling was used to interpret our mechanical data and clarify the role of stylolites on the brittle strength of carbonate rocks.

## 2. Material studied and experimental set-up

### 2.1 Material origin and preparation of the samples

In this study, we focused on Oxfordian limestones from the Eastern part of the Paris Basin. Several boreholes were drilled surrounding the ANDRA (French agency for nuclear waste disposal) Underground Research Laboratory (URL) near the town of Bure, France. All the limestones studied here are from the same borehole (EST205) and belong to units located above the URL, which is built within a layer of claystone (see Rolland et al., 2014 for details). Stylolites are abundant in most of the retrieved core (Fig. 1a). The larger stylolites (of centimeter size) were open in all cases, probably due to the depressurization upon retrieval. For this study, we focused on sedimentary stylolites and selected zones presenting regularly spaced closed stylolites surrounded by sufficient reference stylolite-free material to be used for comparison. The typical distance between the studied stylolite and the stylolite-free material was about 10 cm. We avoided zones with large heterogeneities, anostomosing stylolites, and stylolites with tilted teeth. We also disregarded partially open stylolites that we could easily spot from the high resolution pictures of Rolland (2013). Because of these quite restrictive criteria, we could not sample the available cores at regular interval of depths. We focused on 6 different depths between 158 and 364 m. The geological and textural details of these layers, named for simplicity in this study O1 to O6, are given in Table 1, based on the previous systematic study of André (2003). The studied units are grainstones, wackstones, and packstones. The stylolites in these different layers show different morphologies, studied in detail by Rolland et al. (2014). In particular, the amplitude of the teeth was observed to be quite variable, from 1 milimeter (Fig. 1b) to a centimeter and sometimes more (Fig. 1c).

Figure 1

Table 1

Cylindrical samples nominally 4 cm long and 2 cm in diameter with and without stylolites were prepared from the 10 cm diameter cores (Fig. 2a-b). For the samples with stylolites, two

orientations were cored: orthogonal and parallel to the stylolite plane. Where possible, several samples at an oblique orientation (~60°) were also prepared (Fig. 2c). At each selected depth, stylolites with different morphologies were encountered (Rolland et al., 2014). We only grouped results on stylolites that showed common morphological attributes and when possible obtained all the data from the same stylolite. This preparation phase was challenging and coring in three different orientations often minimized the number of cores we could prepare from a given length of core. Further, cutting and drilling into the cores occasionally revealed large heterogeneities, local variations in stylolite orientation, teeth of very high amplitude (with respect to the sample size), and additional stylolites invisible from the surface of the cores. Additionally, some stylolites opened during the sample preparation process. In the end, more than 25% of the prepared samples had to be disregarded.

Figure 2

## 2.2 Experimental procedure

All samples were first dried in vacuum at 40 °C for a minimum of 48 h. In this study we performed "dry" (samples vacuumed at 40 °C for 48 h) and "wet" (samples vacuumed at 40 °C for 48 h and then vacuum-saturated in deionized water and left in the vacuum under water for 48 h) experiments. All the samples were deformed uniaxially until failure at a constant strain rate of $10^{-5}$/s. Saturated samples were deformed in a water bath. More details about the experimental set-up can be found in Heap et al. (2014b). In a large majority of cases, the failure was unstable and the samples could not be retrieved for post-mortem microstructural analysis. However we managed to stop a few experiments before failure. Petrographic thin sections were prepared from these deformed samples.

## 3. Petrophysical and microstructural attributes of the studied carbonates

Detailed petrophysical and microstructural analysis over the whole length of the EST205 borehole was recently provided for the stylolite-free limestones by Regnet et al. (2014), see in particular their Fig. 6. We refer the reader to this study for details on the stylolite-free materials and will only focus in this section on the main microstructural attributes of the studied rocks and on the potential petrophysical differences induced by or associated to the presence of stylolites. Previous studies on the same carbonates revealed that the materials studied are composed of more than 97% calcite with minor percentages of dolomite, quartz and clay (Heap et al., 2014a), also in agreement with Regnet et al. (2014), who reported a composition >99% calcite in their samples from the same borehole. The studied limestones have another common attribute: they are all microporous (Heap et al., 2014a; Regnet et al., 2014). Fig. 3a shows as an illustration a SEM micrograph of horizon O1 where the microporosity appears heterogeneously distributed. The larger pores visible in this image have a diameter of about 10-15 μm (Fig. 3b). All the studied carbonates have a high degree of cementation, as illustrated on horizon O3 (Fig. 3c). No pores larger than 5 μm could be observed in this layer. X-ray Computed Tomography data (CT) were also acquired at a resolution of 4 microns on a 4 mm sample from the same depth (Fig. 4). Even at this high resolution, one cannot resolve individual pores and the porosity is typically concentrated around the ooliths (darker zones in the CT image).

Figure 3

Figure 4

Considering the low percentages of secondary minerals, it is reasonable to estimate the porosity of the samples using simply their dry mass and considering 100% calcite (assuming a calcite density of 2.71 g/cm$^3$). Comparison with He pycnometer measurements on a selection of samples showed an agreement between both estimations within less than 5%. This also

means that the proportion of disconnected porosity, if any exists, is within the error bars of the measurements. For saturated samples, we observed a difference of about 0.01% (on average) between the porosity determined by triple weight and that determined by the dry mass only. It is likely that water failed to saturate all of the very small pores. However, while this imperfect saturation could be an issue for some petrophysical measurements, Schmitt et al. (1994) showed on various rock types that it has virtually no effect on the brittle strength for saturation as low as 20%.

The porosity of our samples was found in the range 0.6 to 0.21. Average porosity for the 6 layers is given in Table 1. We observed that sample porosity decreases with depth (Fig. 5). All the samples with a stylolite were found, independent of the orientation, to be more porous than the stylolite-free host rock. The measured difference in porosity was between 0.01 and 0.03. Higher porosities associated with the presence of stylolites were also reported in several previous studies (Dawson, 1988; Braithwaite, 1989; Raynaud and Carrio-Schaffhauser, 1992; Lind et al., 1994; Heap et al., 2014a). This could be related to the formation of the stylolite, in particular if stylolites are seen as the product of the horizontal linkage and vertical coalescence of numerous pressure-solution seams (Nenna and Aydin, 2011), a scenario that promotes the development of secondary porosity. Other interpretation of these higher porosity zones could be the injection of non-equilibrated fluid if stylolites acted as conduits for flow, or more simply the fact that the stylolites grew preferentially in zones of higher porosity, as suggested for the formation of compaction bands (Vajdova et al., 2012).

Figure 5

We estimated the extent of the larger porosity zone surrounding the stylolites by making porosity measurements at regular intervals (~0.5-1 cm) on several cylindrical columns of 10 cm length. A representative example for the horizon O3 is shown in Fig. 6a. One can see that

177 significantly higher porosity was only observed in the immediate surroundings on the stylolite
178 (~0.5 cm). This means that for a 4 cm length sample cored perpendicular to bedding, as
179 shown in Fig. 2, there will be a significant difference in porosity between the central part of
180 the sample and the sample ends. Mercury injection experiments were also performed on a few
181 selected samples taken from the same column (Fig. 6b). Most of the pore-throats have a
182 diameter < 1 μm. These data also suggest that the average pore-throat diameter increased
183 slightly close to the stylolite.

184 Rolland (2013) presented some P-wave velocity data and specific area measurements on the
185 same carbonate layers. These data did not reveal any systematic variations in the vicinity of
186 the stylolite. This confirmed our visual and microstructural observations that the higher
187 porosities measured close to the stylolite were not due to microcracking.

188 Previous studies on stylolites also stressed that they are expected to have a complex internal
189 structure due to the hierarchical nature of their formation, combined with the impact of grain-
190 scale heterogeneities (Ebner et al., 2010) and to the inhomogeneous stress distribution
191 surrounding geometric asperities (Zhou and Aydin, 2010). The first order consequence of this
192 complexity is that the stylolite and its surroundings are also more heterogeneous than the host
193 rock.Fig. 7a shows the tortuous path of a stylolite in layer O3. While the stylolites are visible
194 on the sample surface, they are more challenging to follow at smaller scale and in fact it is
195 their complex and heterogeneous nature, with grain partially dissolved (Fig. 7b), that reveals
196 them in optical and SEM micrographs..

197 Figure 6

198 Figure 7

199

200 **4. Mechanical data**

We performed 48 uniaxial tests in total, including 32 on samples with a stylolite. Representative stress-strain curves are presented in Fig. 8. For reasons explained earlier, we had to disregard a fair number of samples and this is why we cannot provide a complete set of dry and wet experiments for all the orientations and all the layers. When we anticipated that testing all the orientations would not be possible, we used the remaining parts of the cores to duplicate certain tests and appreciate the repeatability of the results.

We observed that the Uniaxial Compressive Strength (UCS) of the stylolite-free limestone is in the range 48-150 MPa in dry conditions and 30-90 MPa in wet conditions. The stylolite free material did not show any evidence of mechanical anisotropy, as it can be seen on Fig. 8f for O3. This is perhaps not unexpected since Rolland (2013) and Heap et al. (2014a) did not measure any anisotropy of P-wave velocity and permeability on the same rocks, respectively.

As far as the impact of stylolites is concerned, the main features that can be seen in Fig. 8 and are the following:

- The stress-strain curves of the samples with a stylolite and the stylolite-free samples did not show any significant differences, and both were typical of what is usually observed in this type of uniaxial experiment: after an elastic (linear) stage, the curves reach a peak beyond which strain softening and unstable failure occur. We note however that the failure appeared more unstable when the stylolite was oriented parallel to the applied stress.
- All the samples with a stylolite are weaker than the corresponding stylolite-free samples.
- The difference in strength between the samples with a stylolite and the stylolite-free samples is about the same in dry and wet conditions.

- In all tested horizons, the presence of a stylolite did not induce any mechanical anisotropy and the UCS was about the same for samples with a stylolite oriented orthogonal, parallel, or oblique to the direction of the applied stress (vertical).
- In most cases, the tangent modulus of the samples with a stylolite was smaller than that of the stylolite-free samples.

Figure 8

## 5. Failure modes and microstructural observations

All the stylolite-free samples failed by axial splitting (Fig. 9a). We managed to stop one of the experiments on layer O3, shortly after the peak stress. As expected, we observed axial microcracking distributed homogeneously in the sample and cutting through the cement and the ooids (Fig. 9b). The failure mode was similar for samples with a stylolite oriented orthogonal to the applied stress. Even if our experimental set-up allowed us to observe the sample during deformation, it was not always possible to spot from where the main fracture initiated. Post-mortem observations of these samples showed that the main macroscopic fracture either cuts through the stylolite plane (Fig. 9c), or occurred in two stages where half of the sample is first broken from one end to the stylolite plane, and then the failure continued seconds later from the same position in the stylolite plane or with some horizontal offset as in the example shown in Fig. 9d. We studied the microstructure of one deformed sample of layer O5 that showed less obvious damage. The SEM micrograph of this sample (Fig. 9e) revealed that part of the axial microcracking initiated from the stylolite plane and in particular from the larger teeth of the stylolite. These observations suggest that in this orientation the stylolite plane (and perhaps its surroundings) acted as a zone of high stress concentration and played a fundamental role in the development of stress-induced damage and failure of the sample.

Figure 9

When the stylolite plane was oriented parallel or oblique with respect to the applied stress, we observed different failure patterns in the different samples. The common attribute was the fact that failure occurred sub-vertically in most samples and some damage was always associated to the stylolite plane. This could be easily verified on the broken samples since the fracture plane appeared dark when it followed on the stylolite plane (cutting through the insoluble layer) and white when the fracture developed outside the stylolite plane. When the stylolite was oriented parallel to the applied stress, visual inspection of the broken samples suggested that the main failure was in all cases strongly influenced by the presence of the stylolite (Fig.10). When the stylolite was very tortuous, macroscopic cracking cut sub-vertically through its larger (horizontal) teeth, as in the example shown in Fig. 10a. When the stylolite was less tortuous, we often observed only a partial overlap between the stylolite and the failure plane (Fig. 10b), probably due to end effects or/and to the presence of heterogeneities in the sample. We also observed in some cases that failure developed quasi simultaneously in and outside the stylolite plane (Fig. 10c). Fig. 10d-e shows SEM micrographs from a sample of O5 unloaded just after the peak stress. The density of axial microcracks appeared larger in the vicinity of the stylolite. In some cases, sub-vertical microcracks followed the stylolite path (Fig. 10d) and sometimes cut through the larger teeth when the stylolite becomes more tortuous (Fig. 10e).

Figure 10

We had only a few samples with oblique stylolites because their preparation limited considerably the number of available samples in the other orientations from the same stylolite. In the deformed samples with an oblique stylolite, we observed that macroscopic failure occurred for the most part on the stylolite plane, as in the example shown in Fig. 11a. In this orientation, the failure mode was therefore different from the axial splitting seen in other orientations. However, we also typically observed some axial microcracking emanating from

274 the stylolite, creating secondary sub-axial macrofractures (Fig. 11a). SEM microstructural
275 observations made on a sample of deformed O5 just beyond the peak stress confirmed what
276 visual inspection of the samples suggested: when the stylolite is less tortuous, stress-induced
277 damage mostly followed its path (Fig. 11b). However, if when the stylolite was more
278 tortuous, including some sub-horizontal segments, stress induced microcracks were mostly
279 observed in the direction of the applied stress (Fig. 11c).

280 In summary, in all deformed samples with a stylolite, visual inspection and microstructural
281 observations suggested a major influence of the stylolite on stress-induced damage and
282 failure, consistent with our mechanical data showing that the presence of a stylolite always
283 induced weakening (Figure 8).

284 Figure 11

285

286 **6. Stochastic modelling**

287 The analysis of brittle failure is samples containing a stylolite could not be achieved using
288 standard micromechanical modelling (see for example Baud et al., 2014) due to the inherent
289 heterogeneity of these samples (see section 3). One has to therefore rely on numerical
290 modelling for this type of complex problem. In this study, we chose to use the 2D Rock
291 Failure Process Analysis finite element code ($RFPA_{2D}$) developed by Tang (1997) and applied
292 in several previous studies to brittle failure of carbonates (Wong et al., 2006) and, more
293 recently, volcanic rocks (Heap et al., 2014c; 2015). The numerical samples of this study
294 (rectangles 40 mm in length and 20 mm in width) consist of 51, 200 square elements (Fig.
295 12a). Because our carbonates are all microporous, we did not include any macroscopic voids
296 in the numerical samples and assumed that the local strength of the element reflects the
297 presence of micropores. To also reflect material heterogeneity at the element scale, each

298 square is assigned Young's modulus and strength using a Weibull probability distribution
299 function (Weibull, 1951):

300 $$f(\sigma) = \frac{m}{\sigma_0}\left(\frac{\sigma}{\sigma_0}\right)^{m-1} \exp\left[-\left(\frac{\sigma}{\sigma_0}\right)^{m}\right] \qquad (1)$$

301 The statistics for failure involve therefore two parameters: $\sigma_0$ proportional to the mean of the
302 strength distribution and *m* which characterizes the degree of heterogeneity of the material.
303 High values of *m* lead to homogeneous samples, and vice-versa. Linear constitutive laws are
304 considered for each element until failure that can occur in shear and tensile mode.
305 Importantly, when an element fails, it is replaced by the same element with a considerably
306 lower strength and Young's modulus. Further details on the model could be found in Tang
307 (1997), Wong et al. (2006), and Heap et al. (2015).

308 We decided to apply this approach to our data on the layer O3. The first step was to set the
309 model parameters to match our data on the stylolite-free material. Table 2 presents the
310 parameters used for this simple case and Fig. 13a shows the simulated stress-strain curve
311 together with the data. The evolution of damage in this simple case is also shown in Fig. 13b.
312 It is clear that the set of parameters giving such results is by no means unique but this is of
313 little importance in this study since we primarily focused here on the impact of stylolites.

314 The second step was to create numerical samples representative of the samples with a stylolite
315 in the different orientations. Guided by our petrophysical data, we first examined the
316 possibility that the observed mechanical behavior and damage patterns would be mostly due
317 to the fact that the thin stylolite is in the middle of a weaker, more porous zone. We therefore
318 performed a first series of simulations with the geometries shown in Fig. 12c-d. The presence
319 of the stylolite in the samples was modelled by a zone of 5 mm thick, while the rest of the
320 sample has the same properties than the stylolite-free sample. Numerous attempts were made

using these geometries in which we varied the thickness and properties of the "stylolite zone" to yield results comparable to our mechanical data on O3. Of course, the geometries shown in Fig. 12c-d introduced more parameters in the model, but the situation with a stylolite was also more constrained by measured values of the strength and elastic parameters in three orientations. Our parametric study showed that our uniaxial data on O3 could be reasonably approached if one considers that the strength of the stylolite zone is 10% less than that of the stylolite-free sample. The parameters for this case, which we will call Simulation 1 from hereon in, are shown in Table 2. The simulated stress-strain curves and damage evolutions are shown in Fig. 14. Damage development in the simulation when the stylolite is either orthogonal or parallel to the applied stress is very similar to our post-mortem observations on deformed samples (Fig. 14b and c). However, we noted two important discrepancies between the results of Simulation 1 and the data. First, the model always predicted a mild mechanical anisotropy (Fig. 14a) with the oblique orientation being always significantly weaker, in contrast to our data. Second, and clearly related to the previous point, failure for the oblique orientation is predicted to occur solely in the stylolite zone with little damage developing in the rest of the sample (Fig. 14d). Additional simulations with the same geometries, considering a more heterogeneous stylolite zone (decreasing $m$ by 25%) and the same strength as the stylolite-free material, led to results almost identical to those presented in Fig. 14. The conclusion is that the numerical samples considered in Fig. 12c-d are too simple, and the simulations suggested that the stylolite geometry needed to be considered in the simulations.

To check this, we implemented a second series of simulations (Simulations 2) on the numerical samples shown in Fig. 12e-g. This time, we digitized one of the stylolites observed in a sample with a vertical stylolite and rotated this stylolite for the other orientations. We imposed, as in Simulation 1, that the stylolite had the same properties than the stylolite-free, except that its strength was 25% less (Table 2). These geometries did not result in any

346 mechanical anisotropy and the simulated damage patterns are in qualitative agreement with
347 our observations (Fig. 15 b-d). In particular, the failure mode for the oblique stylolite was
348 significantly different than in Simulation 1, due to the stylolite roughness, and failure
349 occurred this time only partially on the stylolite plane (Fig. 15b). Similarly to Simulation 1,
350 keeping the same strength for the stylolite and making it more heterogeneous results in
351 qualitatively similar results. Obviously a weaker and more heterogeneous stylolite with
352 slightly different parameter combinations would also give similar results.

353 In summary, our numerical simulations using the $RFPA_{2D}$ code showed that it is possible to
354 produce results in qualitative and quantitative agreement with our mechanical data and
355 observations on samples with a stylolite, by considering the following ingredients in the
356 simulations:

357 -a stylolite seen as a weaker and/or more heterogeneous zone in a carbonate formation, in
358 agreement with our petrophysical measurements and microstructural observations;

359 -and a certain roughness of the stylolite, which according to the simulations, is the main factor
360 leading to the absence of mechanical anisotropy.

361

362 **7. Discussion**

363 **7.1 Microstructural control of mechanical strength of the limestone from Bure**

364 To provide reference data on the stylolite-free material, we characterized the mechanical
365 behavior of the limestone formations of Oxfordian age located on the top of the ANDRA
366 URL in Bure. We present in Fig. 16 our new dry UCS data against porosity for the stylolite-
367 free samples, together with a compilation of data for allochemical and micritic limestones
368 from Zhu et al. (2010). We first noted that the strength of the carbonates from Bure is in most

369 cases between the compiled data for the allochemical and micritic limestones. This is not
370 unexpected because, if the rocks from Bure are of allochemical origin, they showed a very
371 high degree of cementation and a very small amount (or a total absence) of macropores, see
372 Fig. 3 and 4 and the previous microstructural results of Heap et al. (2014a) and Regnet et al.
373 (2014). This is in contrast to most allochemical limestones compiled in Fig. 16 (see for
374 example the statistics on macroporosity recently presented in Ji et al., 2012 and 2014).
375 Previous microstructural studies showed that the main micromechanism leading to brittle
376 failure in porous limestone is pore-emanated microcracking (Vajdova et al., 2010; 2012). This
377 scenario was captured by Sammis and Ashby's (1986) micromechanical model. In this
378 approach, spherical pores of constant radius are distributed homogeneously in the sample and
379 when loaded beyond a certain stress, microcracks start to develop from the pores, eventually
380 leading to macroscopic failure. Zhu et al. (2010) proposed a polynomial approximation of
381 Sammis and Ashby's (1986) model for the uniaxial compression case which leads to the
382 following simple expression for the UCS:

383 $$UCS = \frac{1.325}{\phi^{0.414}} \frac{K_{IC}}{\sqrt{\pi r}} \qquad (2)$$

384 Where $\phi$ is the porosity, $r$ the pore radius and $K_{IC}$ the toughness of the material. Since the
385 rocks studied here are carbonates, we take $K_{IC}$ ~0.2 MPa.m$^{1/2}$, consistent with the
386 measurementsof Atkinson and Advis (1980). The prediction of Equation (1) for different
387 values of the ratio $K_{IC} / \sqrt{\pi r}$ are presented in Fig. 16 and suggests that the pore-size
388 controlling brittle failure in these rocks is, according to the model, around 15 μm. This value
389 is high with respect to our microstructural observations and CT data (Figs. 3 and 4). It is
390 possible that the spatial distribution of microporosity primarily at the periphery of the ooids
391 (Fig. 4) had some influence on the strength of the rocks and this is not taken into account in
392 the model.

393 Figure 16

394 We observed for all the tested rocks a large water-weakening effect, with in average a
395 reduction of 34% of the UCS in the water-saturated sample. Brantut et al. (2014) recently
396 showed that significant time-dependent deformation due to stress-corrosion microcracking
397 could occur in limestone in the presence of water. Considering that the experiments were
398 performed at relatively large strain rates, we do not believe that this was a factor here and
399 water-weakening had to be related to some time-independent process. Following Equation 1,
400 it is more likely that this weakening effect is due to a reduction of the fracture surface energy
401 (and consequently of $K_{IC}$) in the presence of water as it has been observed in other rocks such
402 as sandstone (Baud et al., 2000) and Tuff (Zhu et al., 2011). Our results suggest that the
403 reduction of the fracture surface energy in the presence of water is more pronounced in
404 limestone than in sandstone. Direct measurements of $K_{IC}$ on dry and wet limestones should be
405 performed to confirm this conclusion. Such work is beyond the scope of this study.

406

407 **7.2 Impact of stylolites on strength**

408 Our new data compiled in Fig. 17 show an average reduction of the UCS of 28% for a sample
409 containing a stylolite. This reduction was however quite variable and was found to be in the
410 range 10 to 60%. Since the studied stylolites were closed, we can consider these numbers as
411 lower bounds for the expected strength reduction associated with the presence of stylolites.
412 The obvious conclusion is that impact of stylolite on strength of carbonates cannot be
413 neglected in various geophysical and geotechnical applications, even if the stylolites are
414 closed. Our new data also suggests that the origin of this weakening is likely to be complex.
415 Larbi (2003) suggested that stylolites have a weakening effect as they allow the water to
416 penetrate into the rock and dissolve some of the constituents in the stylolites, or cause them to
417 swell. However the results presented in Fig. 8 show a similar reduction in strength for both

418 dry and wet samples, ruling out that clay swelling as a factor in our experiments. One
419 unexpected result is the fact that the stylolite orientation had little impact on the strength
420 reduction. One possible explanation would of course be that the stylolites, because they were
421 very thin, did not particularly influence the mechanical behaviour of the sample and that what
422 was observed was only due some petrophysical differences in the vicinity of these structures,
423 either of pre-stylolization origin or in relation to the stylolite nucleation and growth. However,
424 some of our numerical simulations (Simulations 1) showed that it is unlikely to be that simple.
425 Moreover, if we consider that the host rock has a porosity and pore size of $\phi_h$ and $r_h$, and that
426 porosity and pore size around the stylolite is larger: $\phi_s$ and $r_s$, respectively. Assuming for
427 simplicity that the whole sample with a stylolite has these different microstructural attributes,
428 the pore-crack model would predict, assuming that the toughness $K_{IC}$ does not change
429 (Equation 2), a strength reduction $R$ of

430 $$R = \frac{UCS^{s}}{UCS^{h}} = \left(\frac{\phi_h}{\phi_s}\right)\sqrt{\frac{r_h}{r_s}} \qquad (3)$$

431 With the measured porosity differences, Equation 3 shows that an increase of the pore size by
432 more than a factor 2 would be needed to find $R$ in the measured range. Since only a small
433 volume around the stylolite appeared to have different properties, a higher porosity (Fig. 6a)
434 and a higher pore throat size (Fig. 6b), it is clear that the stylolite as a structure had a major
435 influence on stress-induced damage in the samples. This is essentially what we see in our
436 numerical simulations.

437 The conclusion is that the strength reduction and failure modes observed in the presence of
438 stylolites are mostly due to the addition of two effects: more porous and therefore weaker
439 material in the vicinity of the stylolite and in the stylolite itself and, the stylolite as a
440 heterogeneity acting as a stress concentrator in the material. Because the roughness of the

441 stylolite has as shown an important role in the development of damage, as suggested by our
442 simulations (Fig. 15), this parameter is probably the reason why some scattering was observed
443 in the data, with a few samples being significantly stronger or weaker than others . Spatial
444 variation of the stylolite roughness would indeed promote such variability because some
445 significant difference would then exist between the samples obviously prepared from different
446 parts of the cores. We believe that stochastic modeling was probably the best approach to
447 study this problem because of the inherent differences between the samples.

448 Additional complexity could also arise from the presence of microcracks around the stylolite.
449 However we believe that such microcracking would mostly enhance the porosity/strength
450 differences between the stylolite and the host rock, which will not significantly change the
451 results presented in Section 6. This was checked through several series of simulations.

452

453 **7.3 Stylolites: planes of weakness in carbonate formations?**

454 The existence of a plane weakness in a rock implies that the rock is weaker in some
455 orientation (Jaeger et al., 2007). Many examples showed that the brittle strength of rocks is
456 strongly influenced by various geological features such as joints and fractures (Bandis et al.,
457 1983; Pollard and Aydin, 1988), and structural heterogeneities such as bedding in sedimentary
458 rocks or cleavage in slates, and preferred orientation and/or arrangement of minerals and
459 cracks in crystalline igneous and metamorphic rocks (Donath, 1964; Vernik et al., 1992; Baud
460 et al., 2005). In most of these cases, a degree of mechanical anisotropy is observed. In a
461 foliated rock such as gneiss, a minimum strength is usually observed when the foliation plane
462 is orientated at 45° with respect to the major principal stress (Shea and Kronenberg, 1993;
463 Rawling et al., 2002). Similar observations were also reported on shales by Niandou et al.
464 (1997). In crystalline rocks with joints (Jing et al., 1992) anisotropic shear strength was also

observed. In porous sandstone, significant anisotropy can also be associated with sedimentary bedding. For this case, brittle strength decreases relatively continuously between to end-member situations: the rock deformed perpendicular to bedding giving the maximum strength and the rock deformed parallel to bedding giving the minimum strength (Dunn et al., 1973; Gatelier et al., 2002; Bésuelle et al., 2003; Louis et al., 2009). There is paucity of data on the mechanical anisotropy of the limestone but our new data on the rocks from Bure showed that the stylolite-free material is to the first order isotropic. This is also supported by permeability and P-wave velocity measurements on the same rocks (Rolland, 2013; Heap et al., 2014a).

Our new data on the impact of stylolites appears to contradict field/quarry based observations that exposed stylolites as planes of weakness in carbonate formations. The limited data set of Rashed and Sediek (1997) also suggests that the stylolites induced some anisotropy with minimum strength at some 45° with respect to the applied stress. The numerical simulations presented in the previous section do not suggest that the presence of microcracks around or in the stylolites would change the observed behavior and explain the differences between our results and field observations. As noted before, this would most probably just introduce more scattering in the results. A likely more important parameter was the observations made during the sample selection out of the cores from EST205 borehole in Bure: thicker stylolites (with thicknesses larger than 1 cm) were always associated to macrofracturing in the cores (Fig. 18a) and were therefore impossible to test. Moreover, most attempts made to prepare samples with stylolites of thickness larger than 2-3 mm resulted in fractures along the stylolite planes during preparation. In the few cases, where the samples did not actually break during preparation, we could always see some macrocracks associated to the stylolite plane (Fig. 18b) and further manipulations of these samples showed that their mechanical strength was dramatically low (Fig. 18c). We therefore believe that the thickness of the stylolites plays a major role on their impact on rock strength. It is important to specify here that the thickness

490 that we are referring to is the actual thickness of insoluble elements that can be seen by eye.
491 Taken together, our results therefore suggest the following scenario: when stylolites are thin,
492 as in the studied samples, their roughness plays an important role in the mechanical behavior.
493 Stress concentrations near the larger teeth oriented in the direction of the applied stress
494 promote microcracking in that direction whatever the orientation of the stylolite. This process
495 does not promote the development of mechanical anisotropy as shown in Simulations 2
496 (section 6) and these stylolites cannot be considered as planes of weakness. However when
497 the stylolite thickness is of the order of several mm and beyond, what is typically observed is
498 that it becomes less tortuous (Fig. 18a). Then, when loaded, such structure will have the
499 tendency to behave in a similar way than the numerical samples of Simulation 1 and, in turn,
500 stylolites will become obvious planes of weakness and have very low strength when loaded at
501 an angle to their plane.

502

503 Figure 18

504

505 **8. Conclusions**

506 In this study we showed that a significant strength reduction is expected in the presence of
507 stylolites, even if there are thin and closed. Such weakening should be taken into account in
508 geotechnical applications, particularly around the ANDRA URL in Bure, an area where
509 stylolites are abundant in the carbonate formations. Since pressure solution seams and
510 stylolites are not always developed enough to be identified in carbonate rocks, they also could
511 contribute to the scattering in the petrophysical and mechanical data often reported in this
512 rock type (see for example Dautriat et al., 2011).
513 When the stylolites are thin, we showed that the observed weakening is about the same for a
514 dry or a wet rock, and also appeared to be the same for different orientations of the stylolite

515 with respect to the applied stress. Most of the observed strength reduction could be explained
516 by the presence of a higher porosity zone in the vicinity of the stylolite. The stylolite itself
517 plays the role of stress concentrator that influences the development of stress-induced damage
518 and failure mode in the limestone.
519 Together with systematic observations made on the available cores taken from the Bure site,
520 our new data suggests that stylolites would become planes weakness in carbonate formations
521 beyond a certain thickness. Our observations suggest that this thickness is around 5 mm and
522 that a more dramatic weakening is to be expected when the stylolite reaches this thickness.
523 Mechanical tests on such thick stylolites were not possible in this study and we believe that
524 they would be extremely challenging to perform. It is in our view more realistic to envisage
525 some indirect *in situ* measurements to quantify strength for thick stylolites and their impact at
526 various scales.
527

528 **Acknowledgements**

529 Data will be available on demand. This work was partially funded by ANDRA through a Ph.D
530 grant for Alexandra Rolland. We thank Bertrand Renaudier and Jean-Daniel Bernard for their
531 very delicate work on the sample preparation. We have benefitted from discussions with
532 Philippe Landrin, François Renard and Teng-fong Wong. We thank Gilles Morvan for his
533 assistance on the SEM.
534

535 **References**

536 André, G., 2003. Caractérisation des déformations méso-cénozoïques et des circulations de
537 fluides dans l'Est du Bassin de Paris, thesis, Univ. Henri Poincaré, Nancy, France.

538 Atkinson, B.K., Advis, V., 1980. Fracture mechanics parameters of some rock-forming
539 minerals determined using an indentation technique. Int. J. Rock Mech. Min. Sci. &
540 Geomech. Abst., 17, 383-386.

541 Bandis, S.C., Lumsden, A.C., Barton, N.R., 1983. Fundamentals of rock joint deformation,
542 Int. J. Rock Mech. Min. Sci., 20(6), 249-268.

543 Baron, M., Parnell, J., 2007. Relationships between stylolites and cementation in sandstone
544 reservoirs: Examples from the North Sea, U.K. and East Greenland. Sed. Geol., 194(1–2), 17–
545 35.

546 Bathurst R.G.C., 1971. Carbonate sediments and their diagenesis. Amsterdam/London/New
547 York: Elsevier.

548 Baud, P., Wong, T.-f., Zhu, 2014. Effects of Porosity and Crack Density on Compressive
549 Strength of Rocks, Int. J. Rock Mech. Min. Sci., 67, 202-211, 2014.

550 Baud, P., Louis, L., David, C., Rawlings, G.C., Wong T.-f., 2005. Effects of bedding and
551 foliation on mechanical anisotropy, damage evolution and failure mode, Geophys. Soc.
552 London Spec. Pub., 245, 223-249.

553 Baud, P., Zhu, W., Wong, T.-f., 2000. Failure mode and weakening effect of water on
554 sandstone, J. Geophys. Res., 105, 16371-16390.

555 Bésuelle, P., Baud, P., Wong, T.-f., 2003. Failure mode and spatial distribution of damage in
556 Rothbach sandstone in the brittle-ductile transition. Pure Appl. Geophys. 160, 851-868.

557 Brantut, N., Heap, M.J., Baud, P., Meredith, P.G., 2014, Mechanisms of time-dependent
558 deformation in porous limestone, J. Geophys. Res., 119(7), 5444-5463.

559 Croizé, D., Renard, F., Gratier, J.-P., 2013. Chapter 3- Compaction and porosity reduction in
560 carbonates: A review of observations, theory and experiments, Advances in Geophysics, 54,
561 181-238.

562 Dautriat, J., Gland, N., Dimanov, A., Raphanel, J., 2011. Hydromechanical behavior of
563 heterogeneous carbonate rock under proportional triaxial loading, J; Geophys. Res., 116,
564 doi:10.1029/2009JB000830.

565 Donath, F.A., 1964. Strength variation and deformational behaviour in anisotropic rock, in
566 State of Stress in the Earth's Crust, edited by W. R Judd, pp. 281-297, New York: American
567 Elsevier.

568 Dunn, D.E., LaFountain, L.J., Jackson, R.E., 1973. Porosity dependence and mechanism of
569 brittle fracture in sandstones. J. Geophys. Res., 78, 2403-2417.

570 Dunnington, H. V., 1967. Aspects of diagenesis and shape change in stylolitic limestone
571 reservoirs, Proc. World Pet. Congr. 7th, Mexico, 2, 339-352.

572 Ebner, M., Piazolo, S., Renard, F., Koehn, D., 2010, Stylolite interfaces and surrounding
573 matrix material: Nature and role of heterogeneities in roughness and microstructural
574 development. J. Struct. Geol., 32(8), 1070-1084.

575 Gatelier, N., Pellet, F., Loret, B., 2002. Mechanical damage of an anisotropic porous rock in
576 cyclic triaxial tests. Int. J. Rock Mech. Min. Sci., 39, 335-354.

577 Heald, M.T., 1955. Stylolites in Sandstones. J. Geol., 63(2), 101-114.

578 Heap, M.J., Baud, P., Reuschlé, T., Meredith, P.G., 2014a. Stylolites in limestones: Barriers
579 to fluid flow?, Geology, 42 (1), 51-54.

580 Heap, M., Petrakova, L., Lavallée, Y., Baud, P., Varley N.R., and Dingwell, D.B., 2014b,
581 Microstructural controls on the physical and mechanical properties of edifice-forming
582 andesites at Volcan de Colima, Mexico, J. Geophys. Res., 119, doi:10.1002/2013JB010521.

583 Heap, M.J., Xu, T., Chen, C-f., 2014c. The influence of porosity and vesicle size on the brittle
584 strength of volcanic rocks and magma, Bull. Volcano., 78:856.

585 Heap, M. J., T. Xu, A. R. L. Kushnir, B. Kennedy, and C.-f. Chen, 2015. Fracture of magma
586 containing overpressurised pores. *Journal of Volcanology and Geothermal Research*, 301,
587 180-190.

588 Jaeger, J.C., Cook, N.G.W., Zimmerman, R.W., 2007. Fundamentals of Rock Mechanics, 4th
589 ed., 475 pp., Blackwell, Oxford.

590 Ji, Y., Baud, P., Vajdova, V., Wong, T.-f., 2012. Characterization of pore geometry of Indiana
591 limestone in relation to mechanical compaction, *Oil & Gas Science and Technology - Revue*
592 *de l'Institut Français du Pétrole*, DOI: 10.2516/ogst/2012051.

593 Jiang, Q., Feng, X-t., Hatzor, Y. H., Hao, X-j., and Li, S.-j., 2014. Mechanical anisotropy of
594 columnar jointed basalts: an example from the Baihetan hydropower station, China, Eng.
595 Geol., 175, 35-45.

596 Jing, L., Nordlund, E., Stephansson, O., 1992. An experimental study on the anisotropy and
597 stress-dependency of the strength and deformability of rock joints, Int. J. Rock Mech. Min.
598 Sci. Geomech. Abstr., 29, 535-542.

599 Larbi, J.A., 2003, Effect of stylolites on the durability of building stones: two cases studies,
600 HERON, 48 (3).

601 Lind, I., Nykjaer, O., Priisholm, S., Olie, M., Springer, N., 1994. Permeability of stylolite-
602 bearing chalk, J. Petrol. Tech., 46, 986-993.

603 López-Buendía, A.M., Guillem, C., Cuevas, J.M., Mateos, F., Montoto, M., 2013. Natural
604 stone reinforcement of discontinuities with resin for industrial processing, Eng. Geol., 166,
605 39-51.

606 Louis, L., Baud, P., Wong, T.-f., 2009. Microstructural inhomogeneity and mechanical
607 anisotropy associated with bedding in sandstone, Pure Appl. Geophys., 166, 1063-1087.

608 Nelson, R.A., 1981. Significance of fracture sets associated with stylolite zones, Am. Assoc.
609 Petrol. Geol. Bull., 65, 2417–2425.

610 Nenna, F.A., Aydin, A., 2011. The formation and growth of pressure solution seams in clastic
611 rocks: A field and analytical study, J. Struct. Geol., 33, 633-643.

612 Niandou, H., Shao, J.F., Henry, J.P., Fourmaintraux, D., 1997. Laboratory investigation of the
613 mechanical behaviour of Tournemire shale. Int. J. Rock Mech. Min. Sci., 34, 3-16.

614 Nicholson, D.T., and Nicholson, F.H., 2000. Physical deterioration of sedimentary rocks
615 subjected to freeze –thaw weathering, Earth Surf. Proc. Land., 25 (12), 1295-1307.

616 Özvan, A., Dincer, I., Acar, A., 2011. Quality Assessment of Geo-materials for coastal
617 structures (Yumurtalik, Turkey), Marine Geores. Tech., 29, 299-316.

618 Park, W.C., Schot, E. H., 1968. Stylolites: their nature and origin. J. Sed. Petrol., 38(1), 175-
619 191.

620 Pires, V., Silva, Z.S., G, Simão, J.A.R., Galhano, C., Amaral, P.M., 2010. “Bianco di Asiago”
621 limestone pavement – Degradation and alteration study, Construt. Build. Mat., 24, 686-694.

622 Pollard, D.D., Aydin, A.A., 1988, Progress in understanding jointing over the past century:
623 Geological Society of America Bulletin, v. 100, p. 1181-1204

624 Rashed, M.A., Sediek, K.N., 1997. Petrography, diagenesis and geotechnical properties of the
625 El-Rufuf Formation (Thebes Group), El-Kharga Oasis, Egypt, J. Afr. Earth Sc., 25 (3), 407-
626 423.

627 Rawling, G.C, Baud, P., Wong, T.-f., 2002. Dilatancy, brittle strength, and anisotropy of
628 foliated rocks: Experimental deformation and micromechanical modeling, J. Geophys. Res.,
629 107 (10), 1-14, 2002.

630 Regnet, J.B., Robion, P., David, C., Fortin, J., Brigaud, B., Yven, B., 2015. Acoustic and
631 reservoir properties of microporous carbonate rocks: implication of micrite particle size and
632 morphology, J. Geophys. Res., doi:10.1002/2014JB011313.

633 Rolland, A., Toussaint, R., Baud, P., Conil, N., Landrein, P., 2014. Morphological analysis of
634 sedimentary stylolites for paleostress estimation in limestones surrounding the Andra
635 Underground Research Laboratory site, Int. J. Rock Mech. Min. Sci., 67, 212-225.

636 Rolland, A., 2013. Rhéologie, localisation de la déformation et histoire des contraintes dans
637 les calcaires du site de Bure, Thèse de doctorat, Université de Strasbourg.

638 Rolland, A., Toussaint, R., Baud, P., Schmittbuhl, J., Conil, N., Koehn, D., Renard, F.,
639 Gratier, J.-P., 2012. Modeling the growth of stylolites in sedimentary rocks, J. Geophys. Res.,
640 Volume 117 (6), B06403.

641 Rustichelli, A., Tondi, E., Korneva, I., Baud, P., Vinciguerra, S., Agosta, F., Reuschlé, T.,
642 Janiseck, J.M., 201. Bedding parallel stylolites in shallow-water limestone successions of the
643 Apulian Carbonate Platform (central-southern Italy), *Italian J. Geos*., in press.

644 Rutter, E.H., 1983. Pressure solution in nature, theory and experiment, J Geol. Soc., 140, 725-
645 740.

646 Sammis, C.G., Ashby, M.F., 1986. The failure of brittle porous solids under compressive
647 stress states. Acta metall. 34, 511-526.

648 Schmitt, L., Forsans T., Santarelli, F.J., 1994. Shale testing and capillary phenomena, Int. J.
649 Rock Mech. Min. Sci. & Geomech. Abstr., Vol. 31, No. 5, 411-427.

650 Shea, W.T., Kronenberg, A.T, 1993. Strength and anisotropy of foliated rocks with varied
651 mica contents, *J. Struct. Geol., 15*, 1097-112.

652 Schmittbuhl, J., Renard, F., Gratier, J.P., Toussaint, R., 2004. Roughness of stylolites:
653 Implications of 3D high resolution topography measurements, Phys. Rev. Lett. 93 (23),
654 238501, doi:10.1103/PhysRevLett.93.238501.

655 Schultz, R.A., 1995. Limits on strength and deformation properties of jointed basaltic rock
656 masses, Rock Mech. Rock Eng., 28(1), 1-15.

657 Stockdale, P.B., 1943, Stylolites: primary or secondary?, J. Sediment. Petrol. 13, 3–12.

658 Vajdova, V., Baud, P., Wu, L., Wong, T.-f., 2012. Micromechanics of inelastic compaction in
659 two allochemical limestones, J. Struct. Geol., 43, 100-117.

660 Vajdova, V., Zhu, W., Chen T.-M.N., Wong, T.-f., 2010. Micromechanics of brittle faulting
661 and cataclastic flow in Tavel limestone, J. Struct. Geol., 32, 1158-1169.

662 Vernik, L., Lockner, D., Zoback, M.D., 1992. Anisotropic strength of some typical
663 metamorphic rocks from the KTB pilot hole, Germany. Sci. Drill. 3, 153-160.

664 Tang, C., 1997. Numerical simulation of progressive rock failure and associated seismicity,
665 Int. J. Rock Mech. Min. Sci., 34, 249-261.

666 Wong, T.-f., Wong, R.H.C., Chau, K.T., Tang, C.A., 2006. Microcrack statistics, Weibull
667 distribution and micromechanical modeling of compressive failure in rock, Mech. Mat.,
668 38,664-681.

669 Yates, T.J.S., Chakrabarti, B., 1998. Stone Cladding panels: In-Sity Weathering, CRC Press,
670 1998.

671 Zhou, X., Aydin, A., 2010. Mechanics of pressure solution seam growth and evolution. J.
672 Geophys. Res.-Solid Earth 115, 18.

673 Zhu, W., Baud, P., Vinciguerra, S., Wong, T.-f., 2011. Micromechanics of brittle faulting and
674 cataclastic flow in Alban Hills Tuff, J. Geophys. Res., 106, DOI: 10.1029/2010JB008046.

675 Zhu, W., Baud, P., Wong, T.-f., 2010. Micromechanics of cataclastic pore collapse in
676 limestone, J. Geophys. Res., 115, B04405, doi:10.1029/2009JB006610.

677

678 **Figure captions**

679 **Fig. 1.** (A) Photograph of a section of a core from the borehole EST205 from the ANDRA site
680 in Bure, France. Three stylolites are visible on the core of ~50 cm length. High resolution
681 photographs showing the details of a stylolite in layers X (B) and Y(C)

682 **Fig. 2.** Preparation of the samples with a stylolite. (A) Slices of about 10 cm were cut in the
683 cores such as the stylolite is in the middle. (B) We cored in several orientations in this slice
684 (B) to obtain samples with horizontal, vertical and oblique stylolite (C).

685 **Fig. 3.** SEM micrographs showing the microporous nature of the carbonates from Bure: (A)
686 microporosity (A) and maximum pore size ~10 μm (B) in an intact sample of layer O1.
687 Highly cemented structure (C) and smaller pore size (D) in in an intact sample of layer O3.

688 **Fig. 4.** Micro CT data with resolution 4 μm data on an intact sample of the layer O3. No
689 macropore is visible and the microporosity appears larger near the edge of the allochems
690 (dark areas).

691 **Fig. 5.** Porosity stylolite-free samples (red) and samples with a stylolite of carbonates from
692 Bure as a function of depth.

693 **Fig. 6**. (A) Evolution of the porosity of the layer O3 near a stylolite. (B) Mercury injection
694 data for the samples 5 (blue), 9 (red) and 11(green) of the same column: Differential intrusion
695 as a function of pore-throat diameter.

696 **Fig. 7.** (A) Mosaic of optical micrographs showing a stylolite. (B) Mosaic of SEM
697 micrograph showing the details of stylolite in layer O3.

698 **Fig. 8.** Representative mechanical data for uniaxial compression tests performed on
699 carbonates from Bure. Axial stress is presented as a function of axial strain for experiments
700 performed on stylolite free samples (plain lines) and samples with a stylolite (dashed lines).
701 Samples cored orthogonal (Z), parallel (X) and oblique to bedding are presented in blue, red
702 and green, respectively. For samples with a stylolite, triangles indicate the orientation of the
703 stylolite. Dry data are presented on layers O1 (A), O6 (B), O2 (C), O3 (E), O5 (G) and wet
704 data on layers O1 (B), O2 (D), O3 (F), and O5 (H).

705 **Fig. 9.** (A) Photograph of a stylolite-free sample of layer O3 deformed uniaxially under
706 nominally dry conditions and which failed by axial splitting. (B) SEM micrograph of a sample
707 of layer O3 deformed uniaxially just beyond the peak stress: axial microcracks cut through the
708 cement and the allochems. Photographs of deformed samples with a horizontal stylolite
709 (orientation Z): (C) from the layer O5 with axial microcracking cutting through the stylolite
710 and (D) from layer O3 showing a more complex failure mode. (E) SEM micrograph of a

711 sample from layer O5 deformed to the peak stress showing that microcracking initiated from
712 the larger teeth of the stylolite. Uniaxial stress was applied in the vertical direction.

713 **Fig. 10.** Photographs of deformed samples with vertical stylolite (orientation X) from layers
714 O3 (A-B) and O5 (C). SEM micrographs of sample of O5 deformed just beyond the peak
715 stress: (D) axial microcracking following the stylolite, (E) axial microcracking close to the
716 stylolite in a more tortuous zone. Uniaxial tress was applied in the vertical direction.

717 **Fig. 11**. (A) Photograph of a deformed sample of O3 with an oblique stylolite. Failure
718 occurred both in and out of the stylolite plane. SEM micrographs of a sample of O5 with an
719 oblique stylolite deformed just beyond the peak stress: (B) Microcracking following the
720 stylolite, (C) Sub-axial microcracking initiating from a sub-horizontal part of the stylolite.
721 Uniaxial tress was applied in the vertical direction.

722 **Fig. 12.** Numerical samples used in the simulations performed with the RPFA code of (Tang,
723 1997). (A) stylolite free samples, (B-D) samples used for Simulation 1 with a weaker stylolite
724 zone, (E-F) samples used for Simulation 2 with a thin tortuous and weaker stylolite.

725 **Fig. 13.** Results of the simulation for the stylolite free material. (A) Stress as a function of
726 axial strain for the sample O3i of layer O3 and for the numerical simulations. The parameters
727 used in the model are listed in Table 2. (B) Stress-induced damage in the numerical sample.
728 Failure of elements appears red when in tension and black when in shear.

729 **Fig. 14.** Results of the Simulations 1 for a sample with a stylolite (Fig.11B-D) (A) Stress as a
730 function of axial strain as predicted by the simulations with a 10% weaker stylolite zone. The
731 parameters used in the model are listed in Table 2. Stress-induced damage in the numerical
732 samples with stylolite oriented orthogonal (B), oblique (C) and (D) parallel to the applied
733 stress (vertical).

734 **Fig. 15.** Results of the Simulations 2 for a sample with a rough stylolite (see Fig. 12 E-F). (A)
735 Stress as a function of axial strain as predicted by the simulations with a 10% weaker stylolite.
736 The parameters used in the model are listed in Table 2. Stress-induced damage in the
737 numerical samples with stylolite oriented orthogonal (B), oblique (C) and (D) parallel to the
738 applied stress (vertical).

739 **Fig. 16.** Comparison of theoretical predictions with laboratory data on unconfined
740 compressive strength (UCS) of micritic (triangles)and allochemical (squares) limestones
741 compiled by Zhu et al. (2010) and the carbonates from Bure (red circles). Theoretical curves
742 of UCS as a function of porosity for four different values of $K_{IC} / \sqrt{\pi r}$ are plotted.

743 **Fig. 17**. Compilation of UCS data on samples with a stylolite (plain symbols) and stylolite-
744 free (open symbols): (A) nominally dry samples, (B) water saturated samples.

745 **Fig. 18**. (A) Photograph of a core from Bure (10 cm diameter). Fracture of this core occurred
746 along a thick stylolite. (B) Photograph of a sample (4 cm x 2 cm) prepared in a zone with a
747 thick tortuous stylolite. Preparation induced cracking is visible in part of the stylolite plane.
748 This Microcracking made this sample way weaker and it broke mostly on the stylolite plane
749 (C).

A)

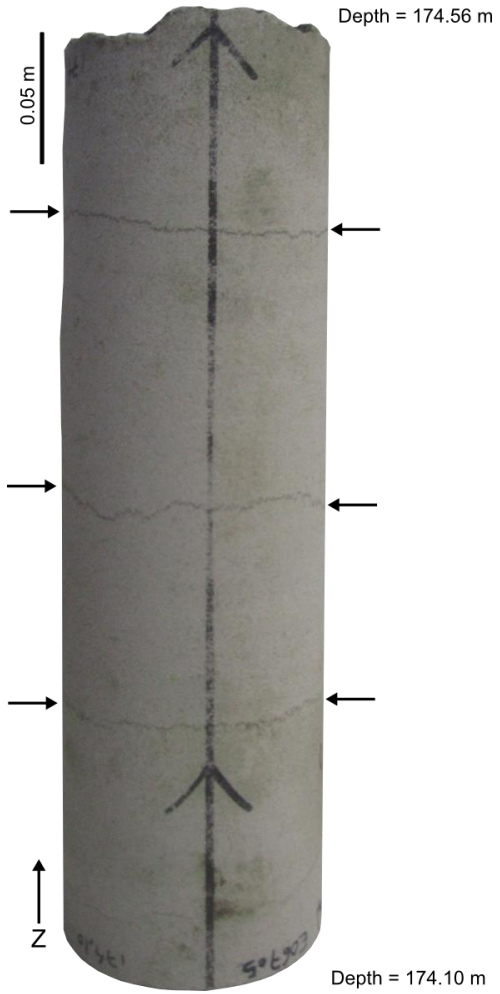


B)

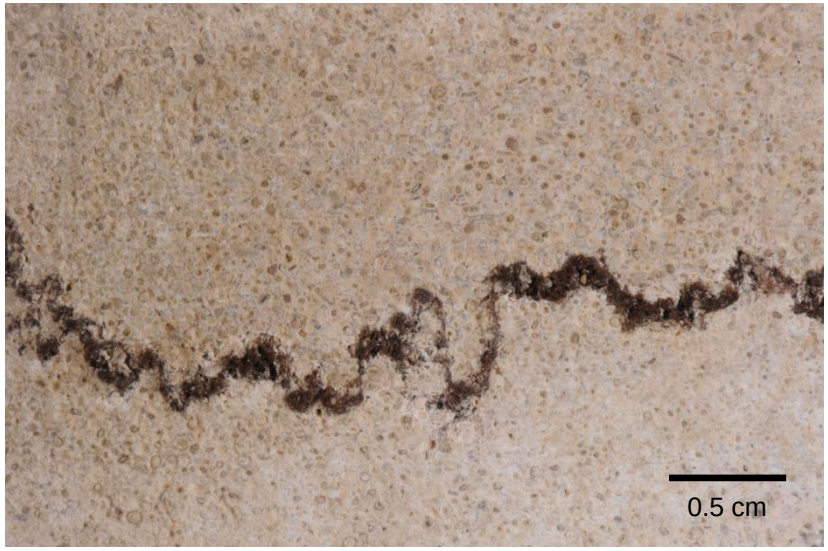


C)


Figure 1

A)

B)

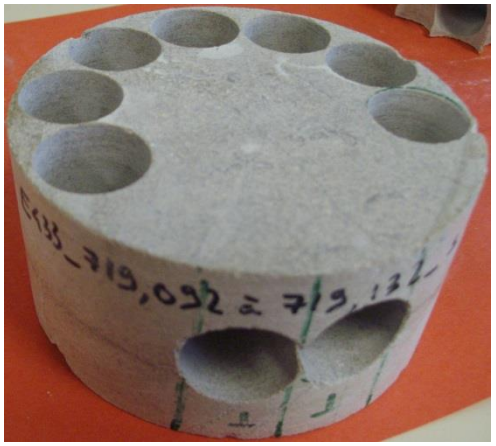

C)

Figure 2

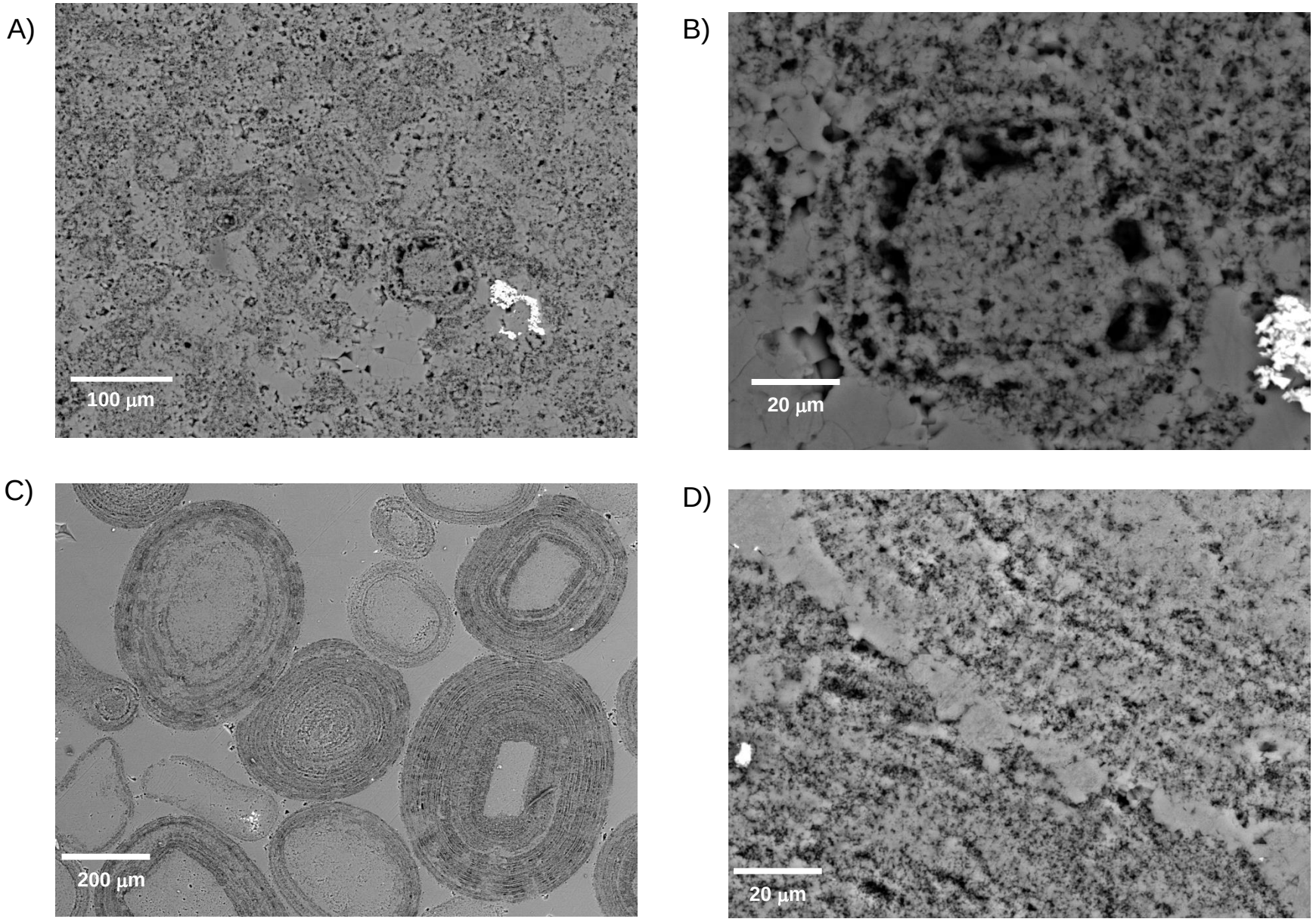


Figure 3

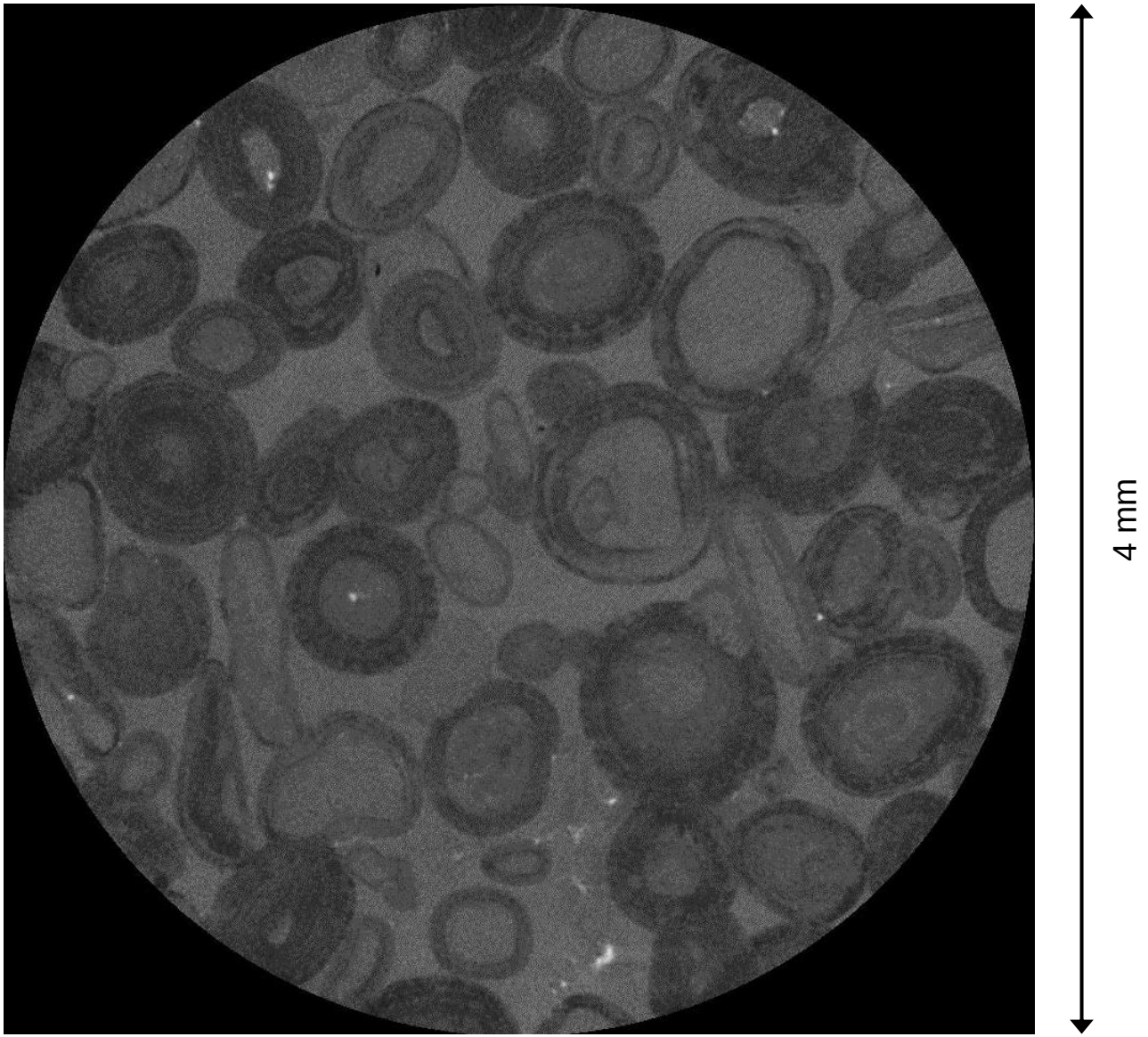


Figure 4

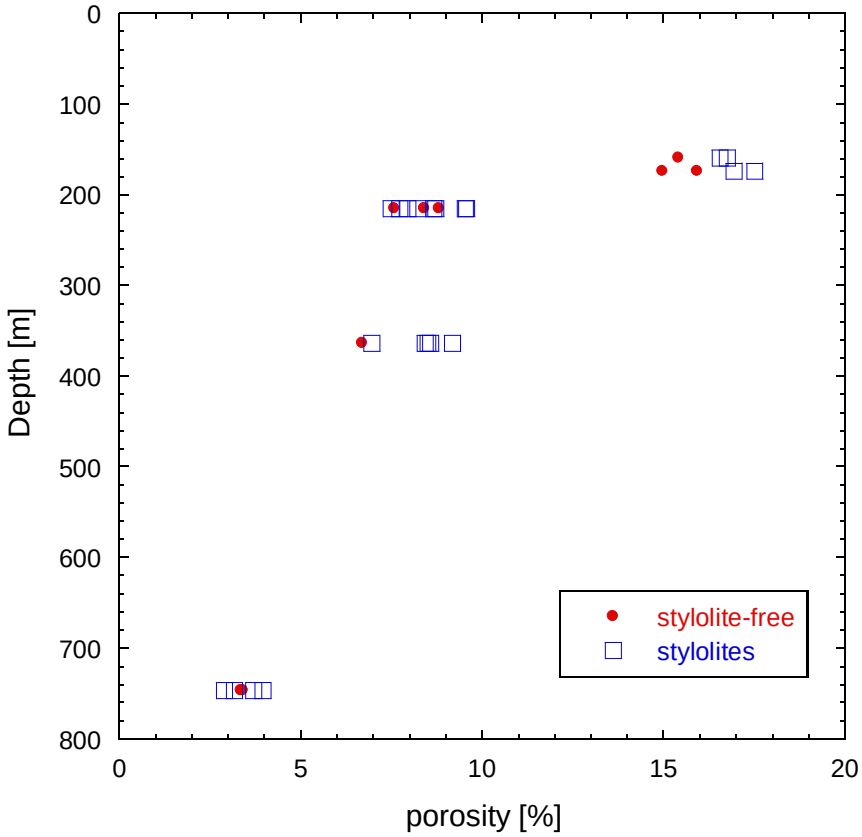
0
100
200
300
400
500
600
700
800
Depth [m]
0
5
10
15
20
porosity [%]
stylolite-free
stylolites

Figure 5

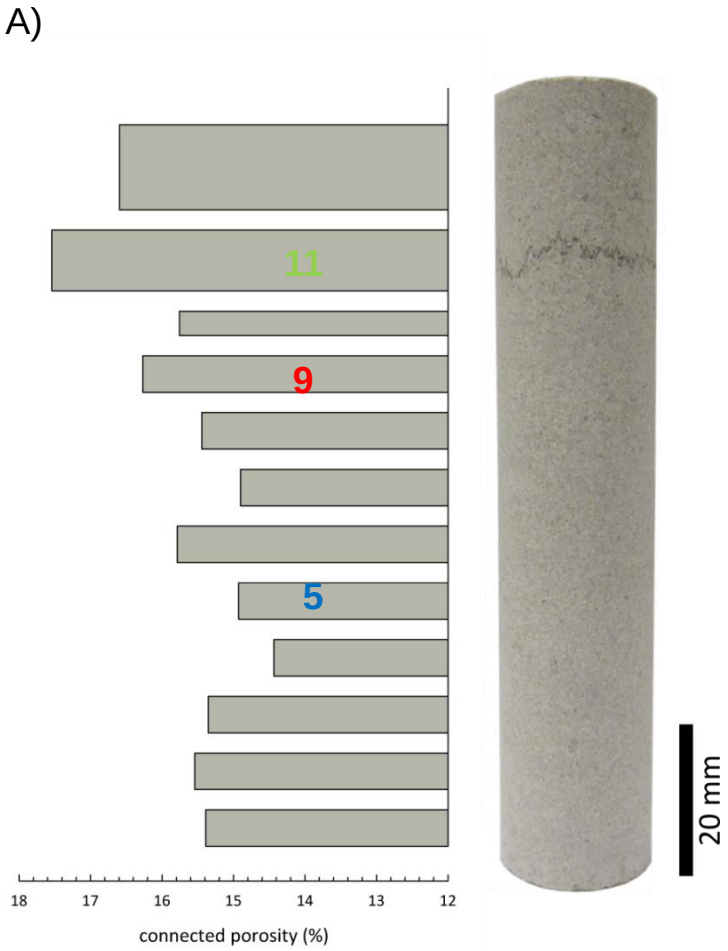
A)
11
9
5
18
17
16
15
14
13
12
connected porosity (%)
20 mm
B)
5
9
11
0.25
0.2
0.15
0.1
0.05
0
Differential intrusion [ml/g]
0.01
0.1
1
Pore-thorat diameter [μm]

Figure 6

A)

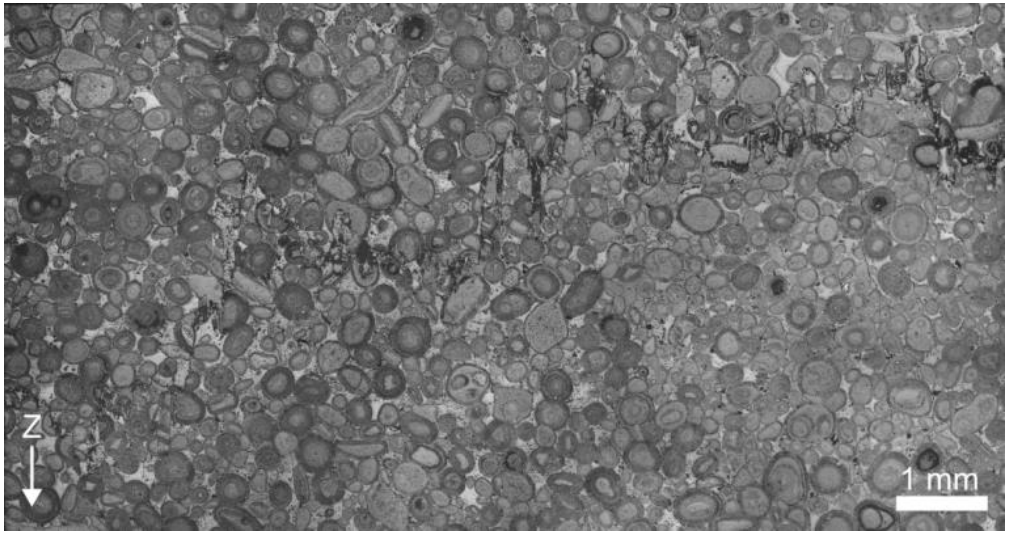


B)

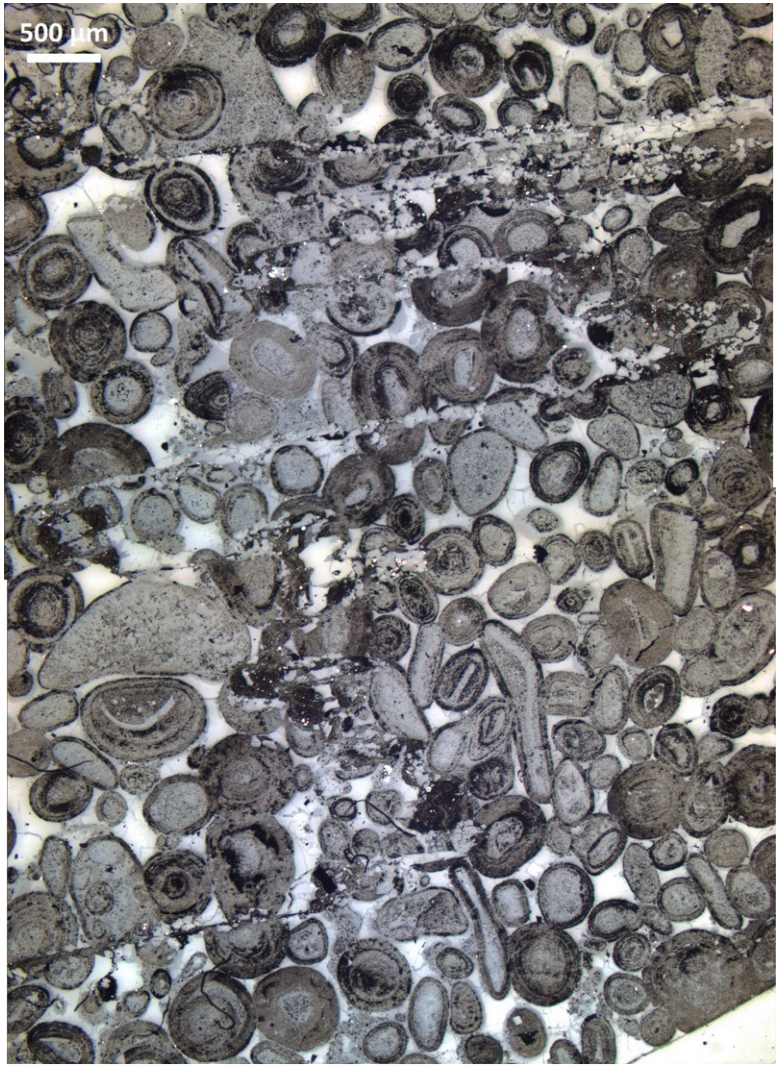


Figure 7

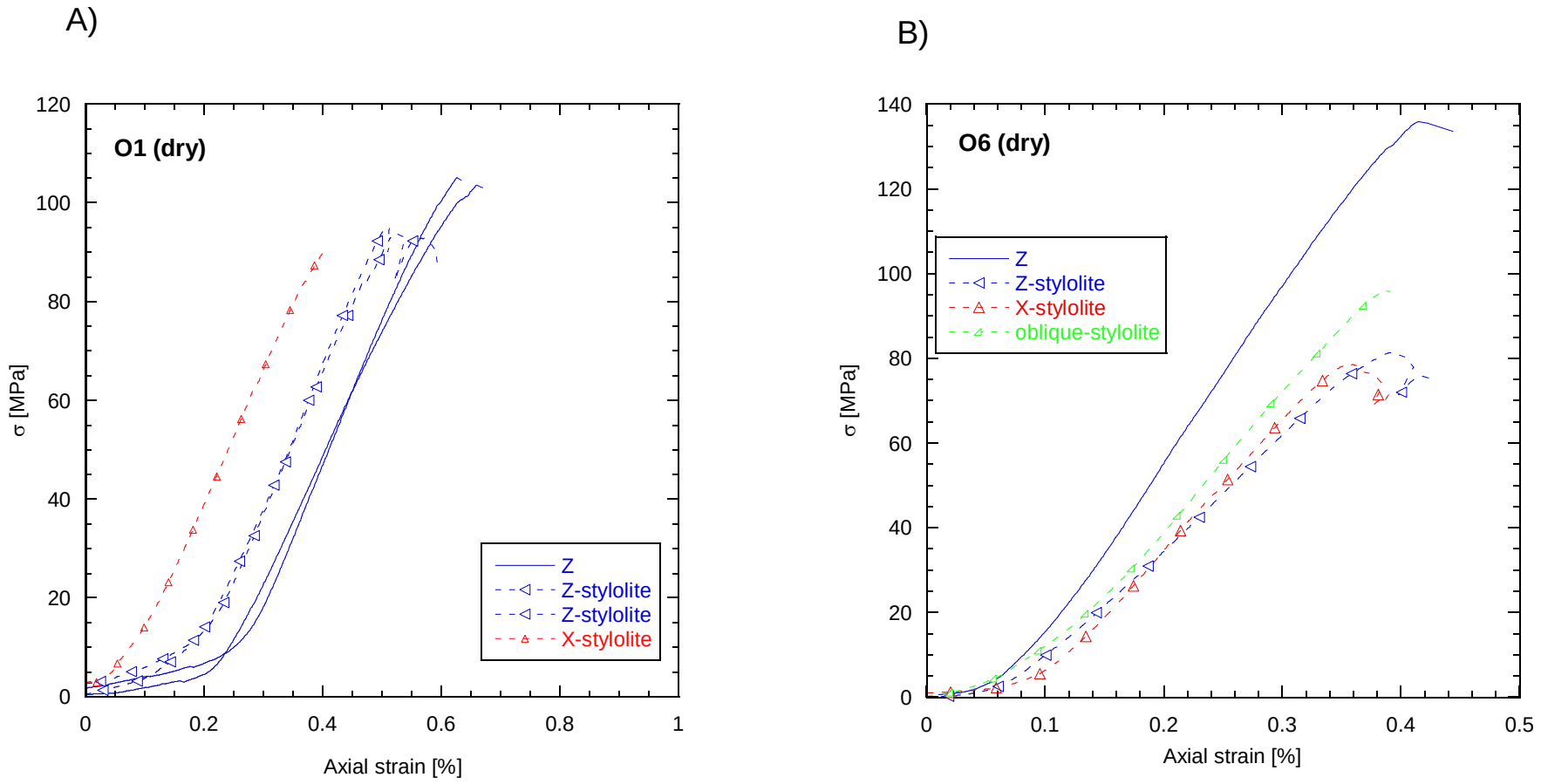
A)
O1 (dry)
σ [MPa]
Axial strain [%]
Z
Z-stylolite
Z-stylolite
X-stylolite
B)
O6 (dry)
σ [MPa]
Axial strain [%]
Z
Z-stylolite
X-stylolite
oblique-stylolite

Figure 8

C)

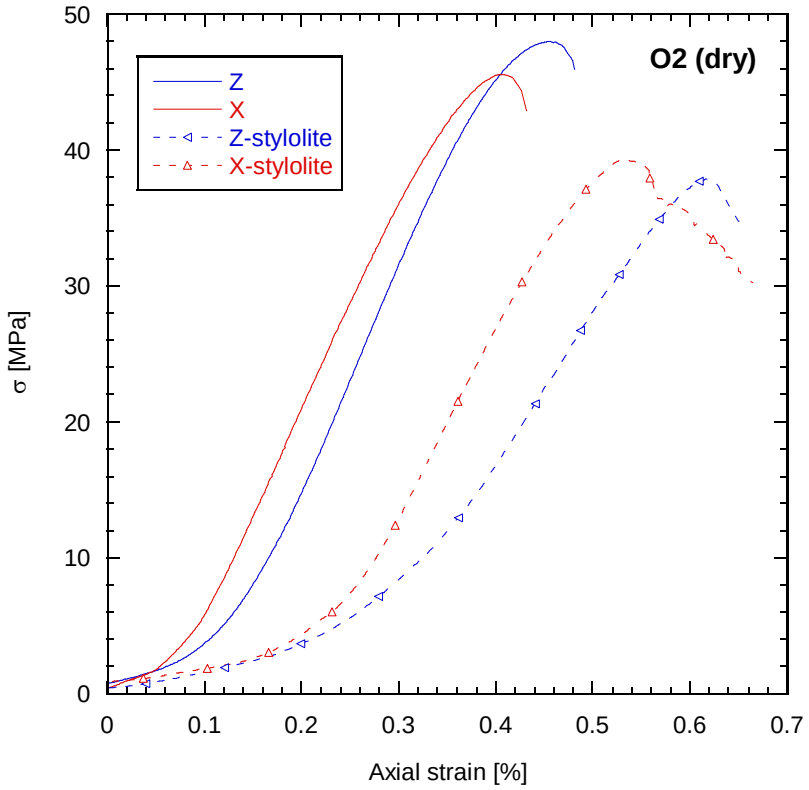
O2 (dry)
Z
X
Z-stylolite
X-stylolite
σ [MPa]
Axial strain [%]
0
10
20
30
40
50
0
0.1
0.2
0.3
0.4
0.5
0.6
0.7

D)

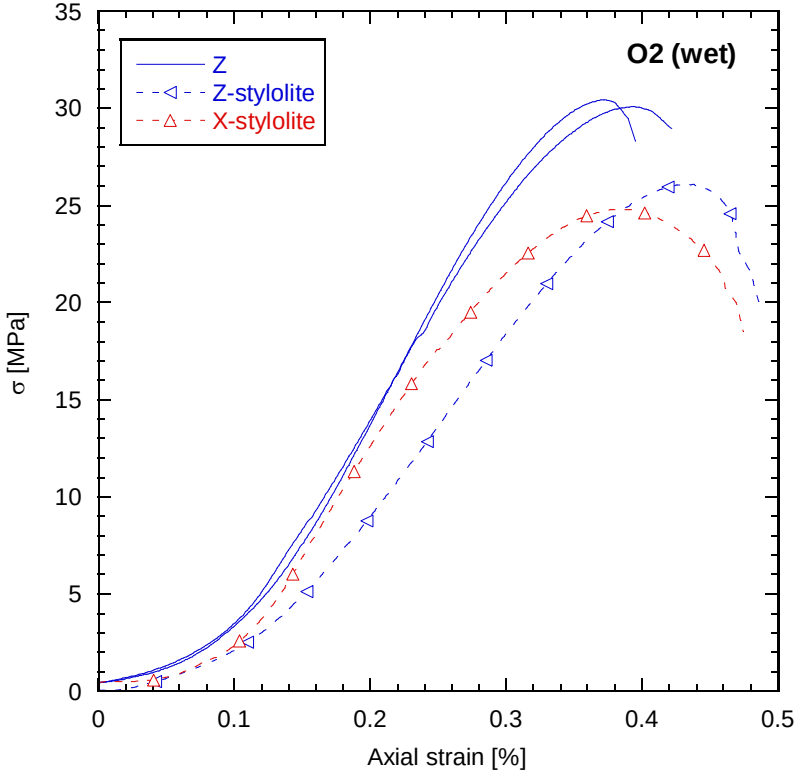
O2 (wet)
Z
Z-stylolite
X-stylolite
σ [MPa]
Axial strain [%]
0
5
10
15
20
25
30
35
0
0.1
0.2
0.3
0.4
0.5

E)

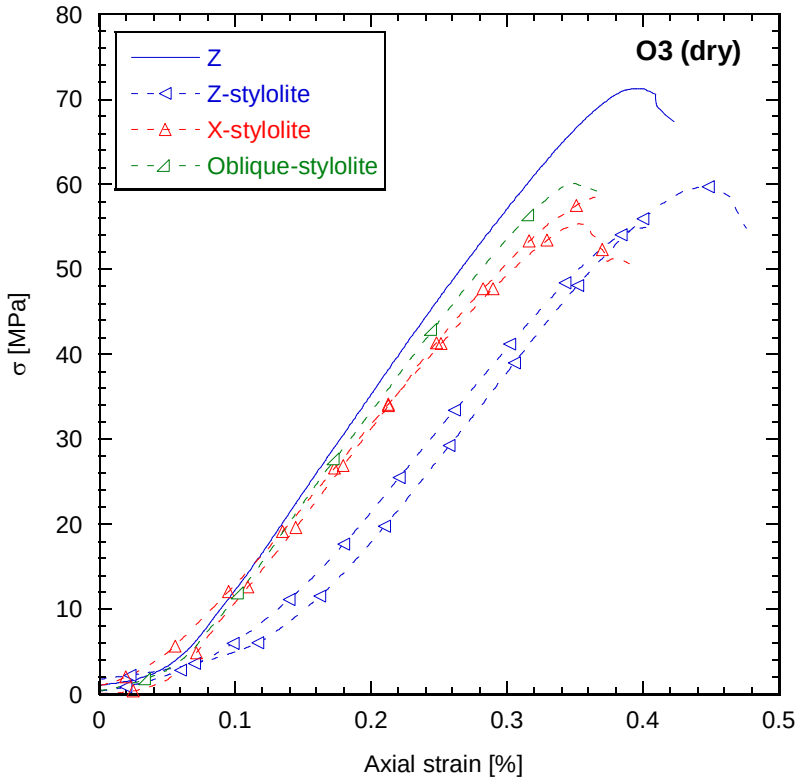
O3 (dry)
Z
Z-stylolite
X-stylolite
Oblique-stylolite
σ [MPa]
Axial strain [%]
0
10
20
30
40
50
60
70
80
0.1
0.2
0.3
0.4
0.5

F)

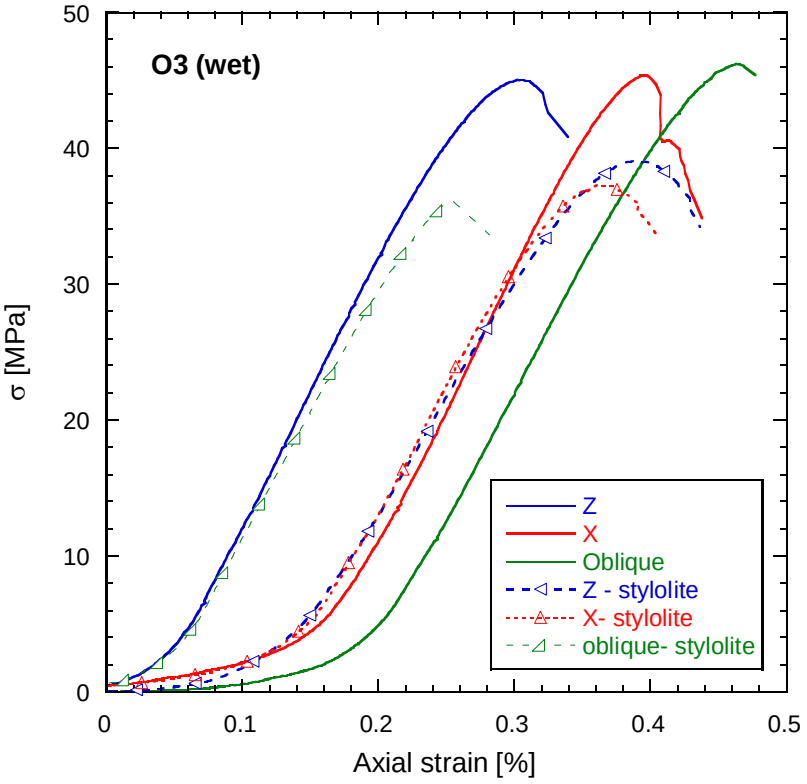
O3 (wet)
Z
X
Oblique
Z - stylolite
X- stylolite
oblique- stylolite
σ [MPa]
Axial strain [%]
0
10
20
30
40
50
0.1
0.2
0.3
0.4
0.5

G)

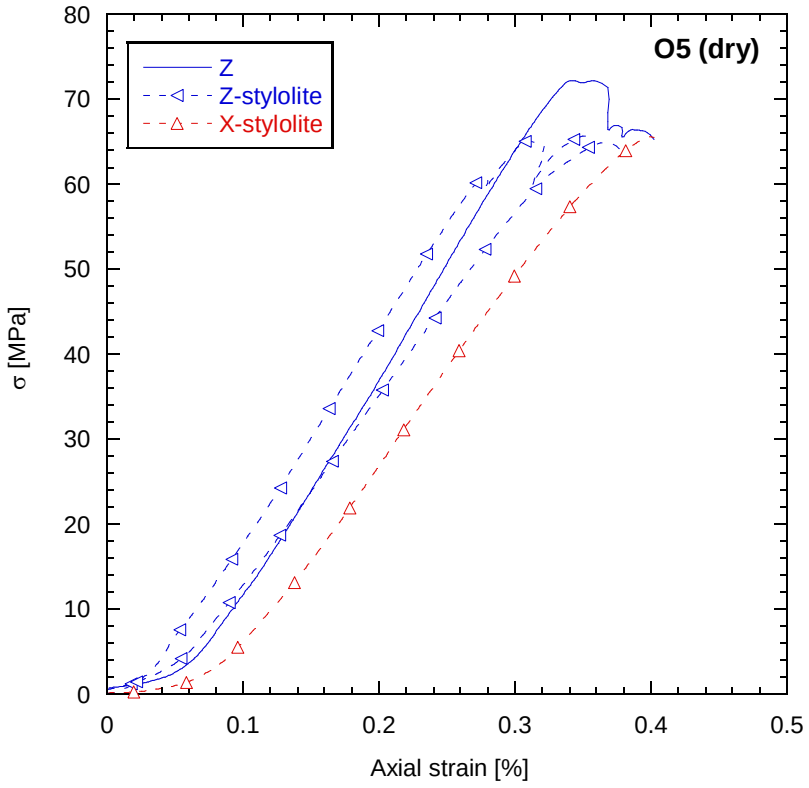
O5 (dry)
Z
Z-stylolite
X-stylolite
σ [MPa]
Axial strain [%]
0
10
20
30
40
50
60
70
80
0
0.1
0.2
0.3
0.4
0.5

H)

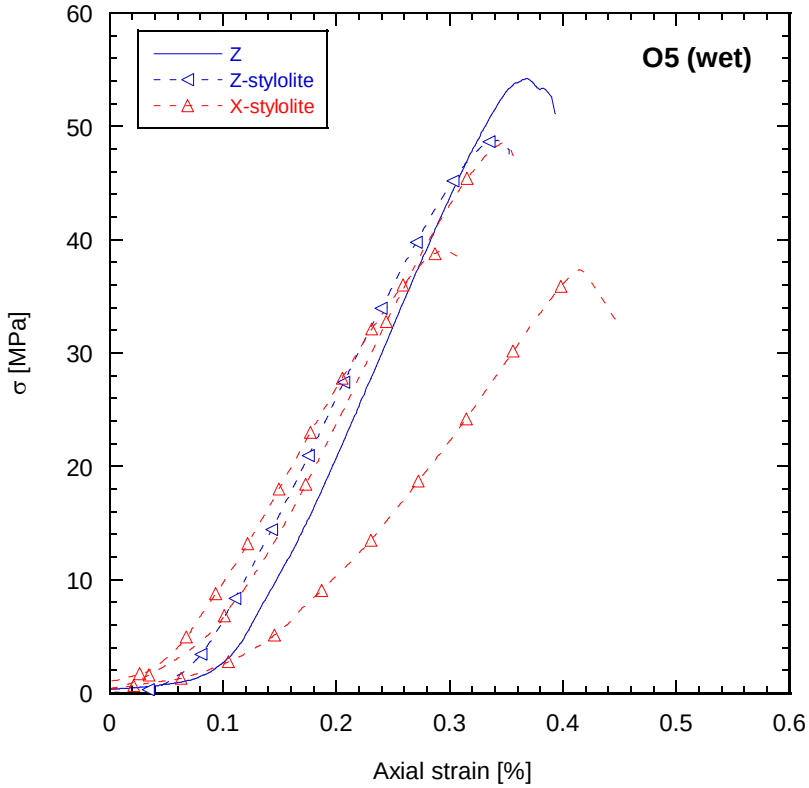
O5 (wet)
Z
Z-stylolite
X-stylolite
σ [MPa]
Axial strain [%]
0
10
20
30
40
50
60
0
0.1
0.2
0.3
0.4
0.5
0.6

A)

B)

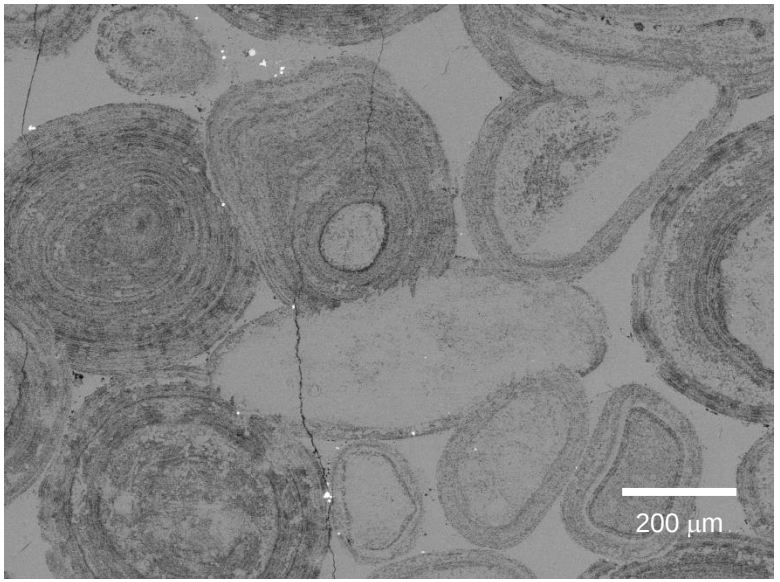


C)


D)

E)

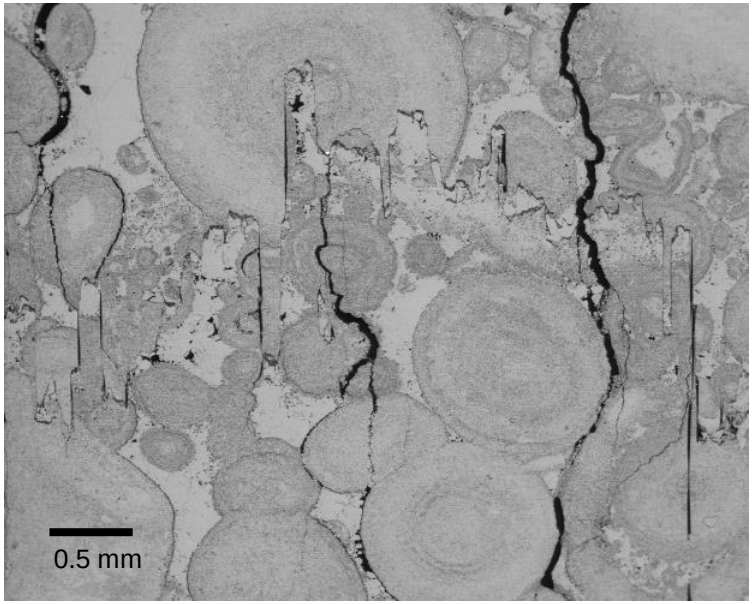


Figure 9

A)

B)

C)

D)

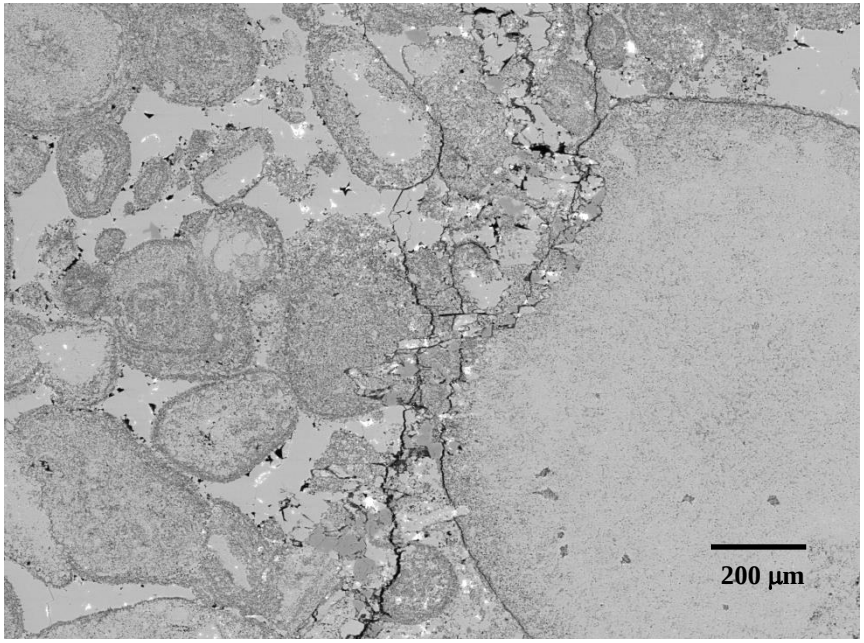


E)

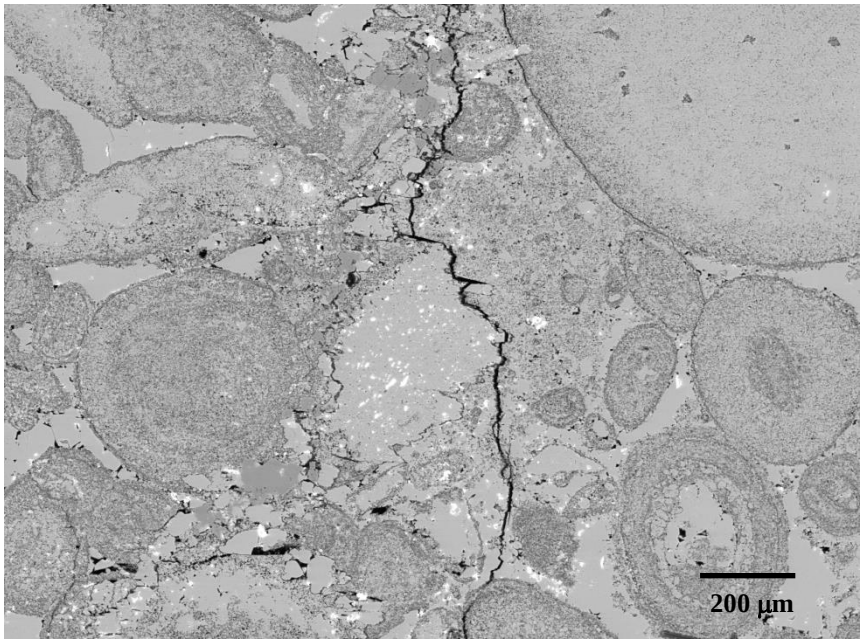


Figure 10

A)

B)

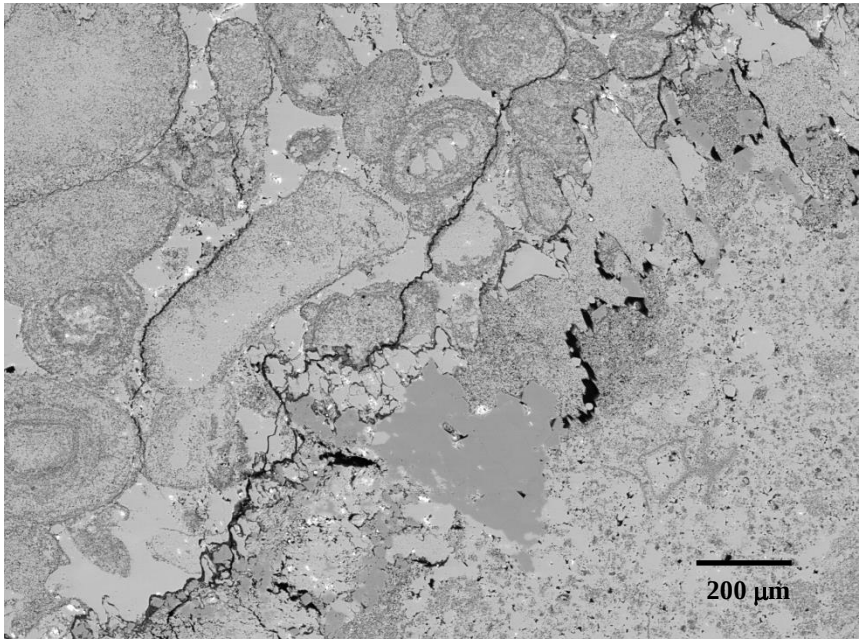


C)

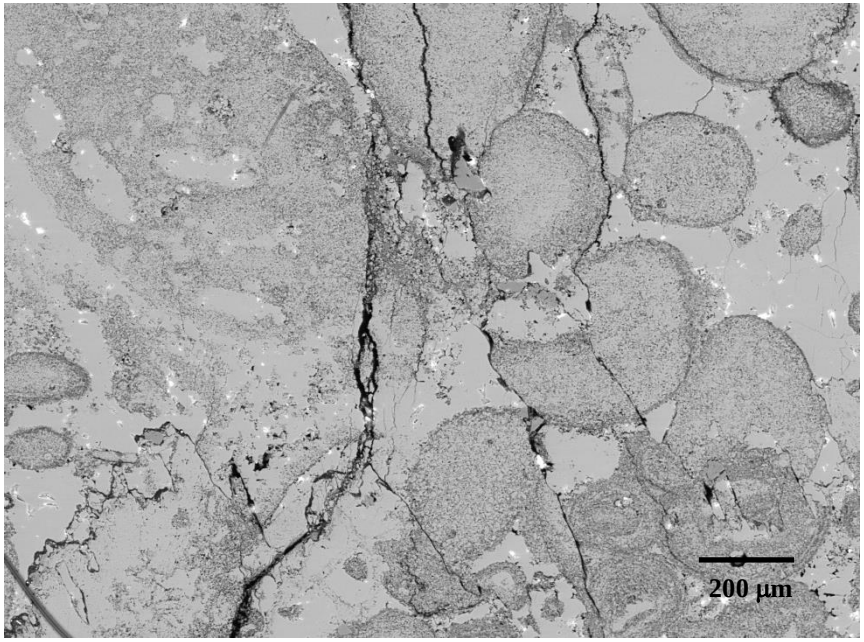


Figure 11

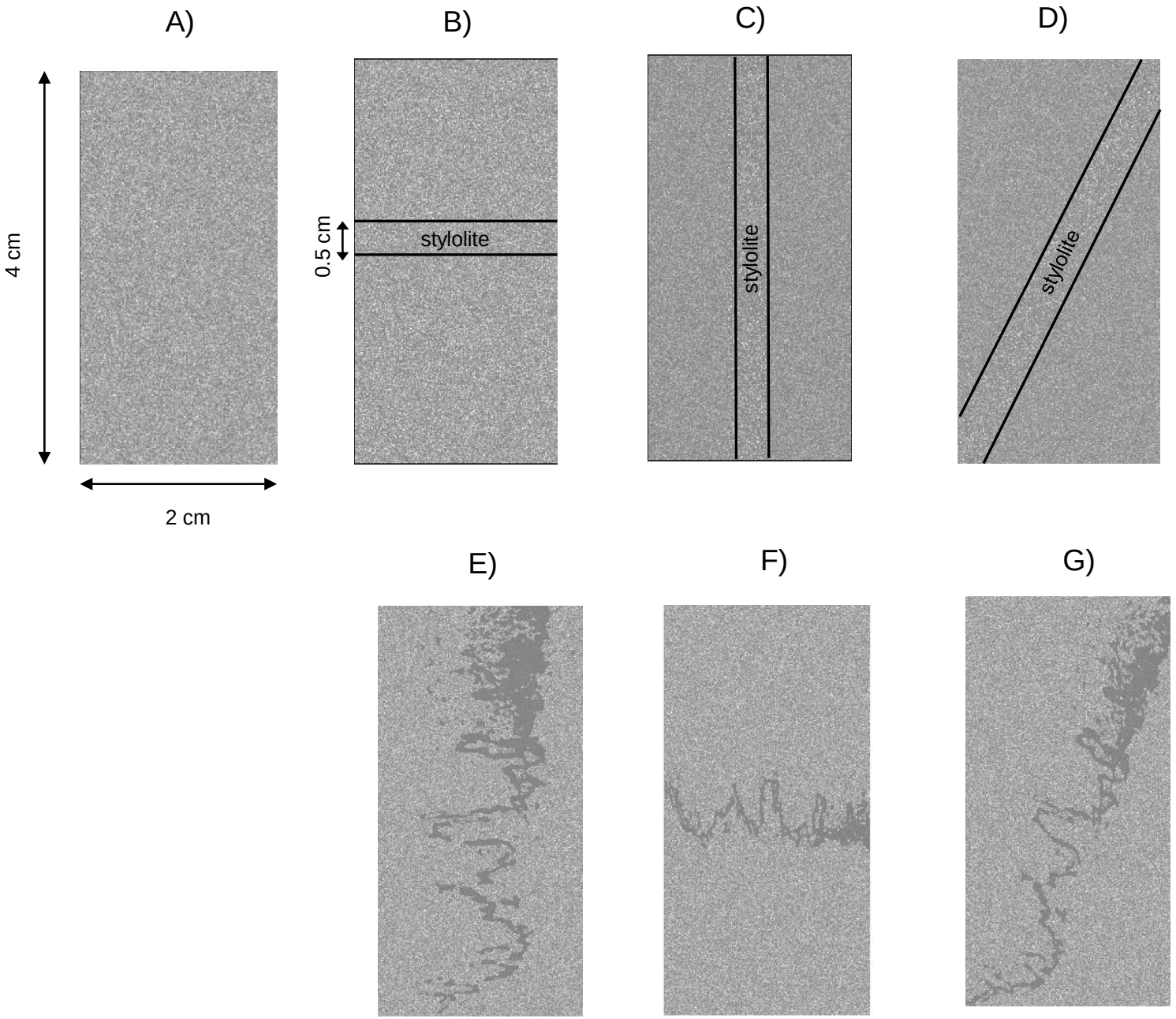


Figure 12

A)

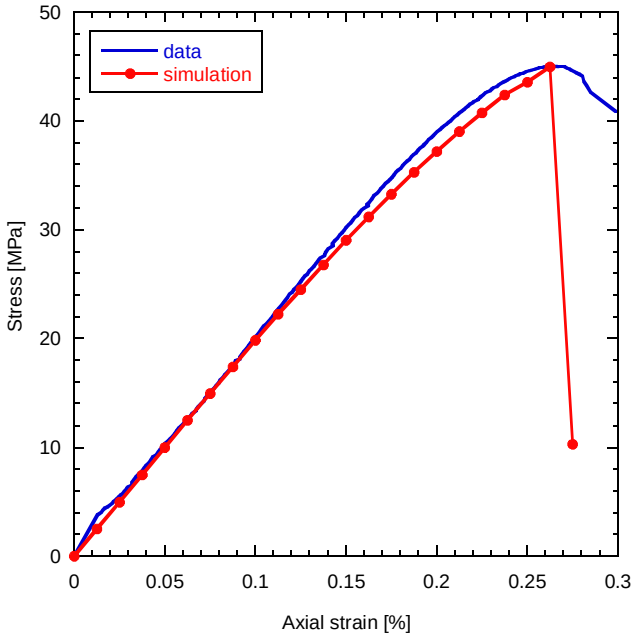


B)

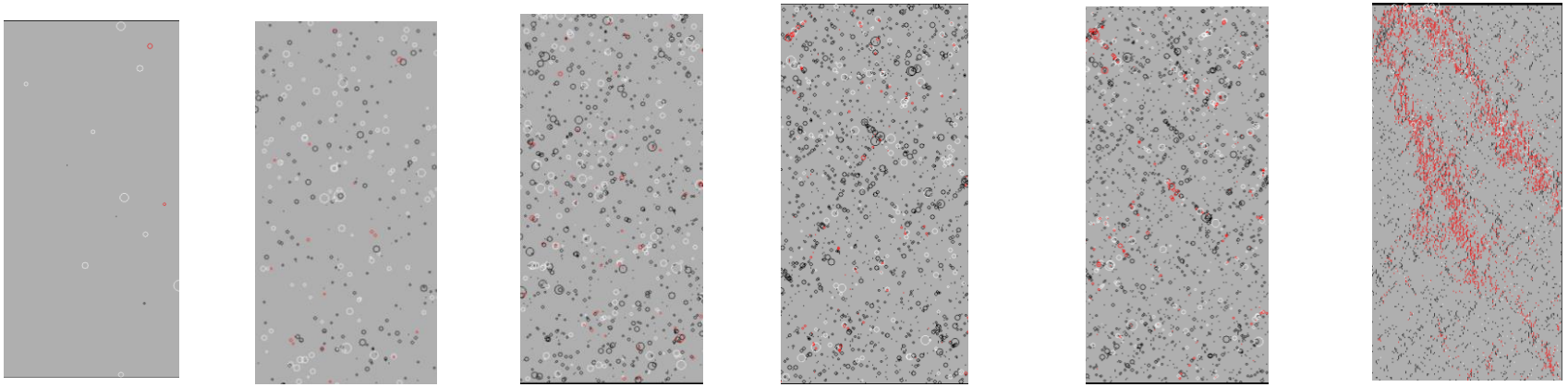

0.08% 0.13% 0.18% 0.23% 0.25% 0.28%

Figure 13

A)

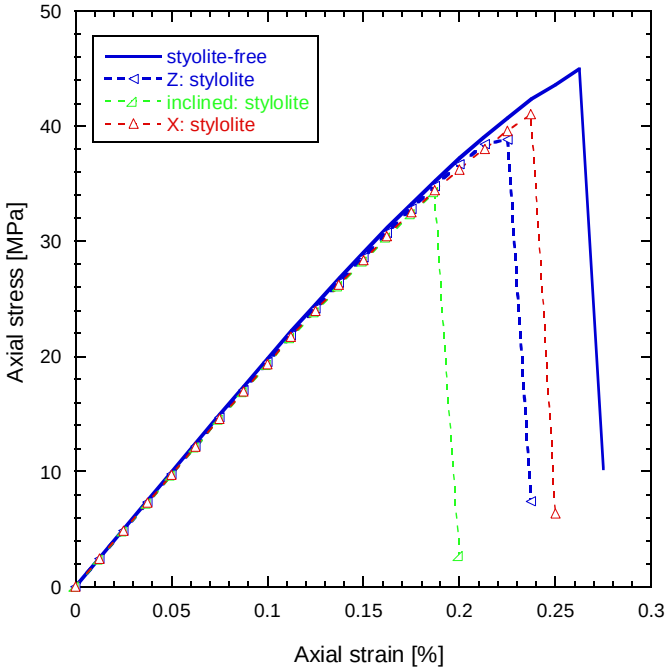


B)

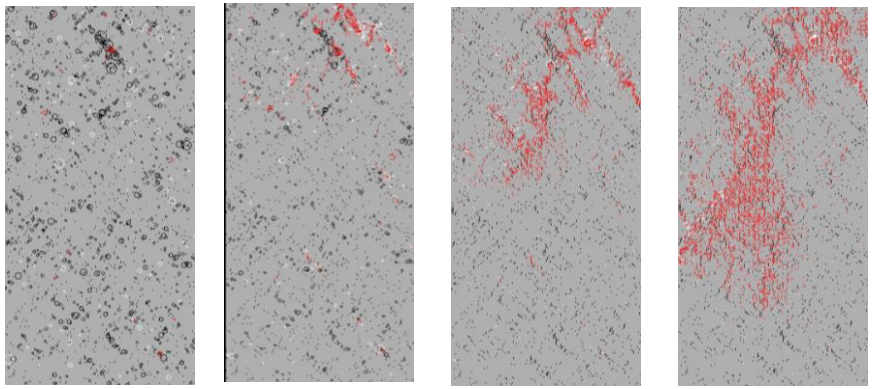


C)

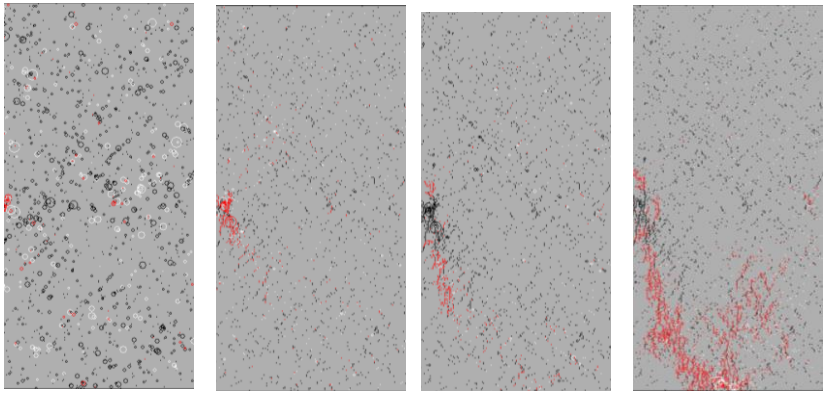


Figure 14

D)

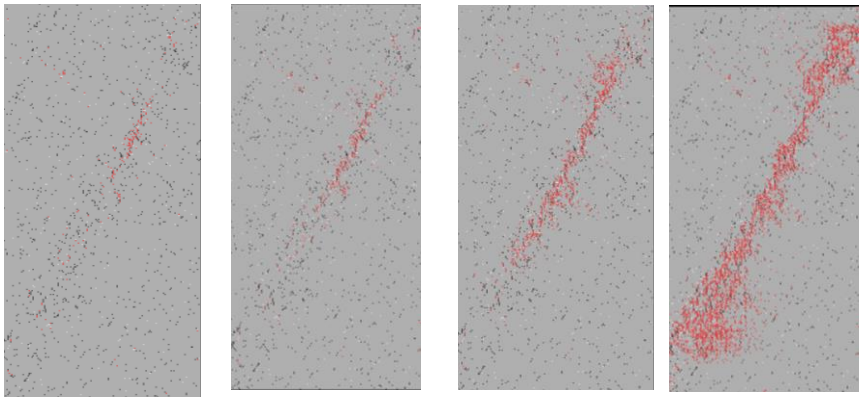


Figure 14

A)

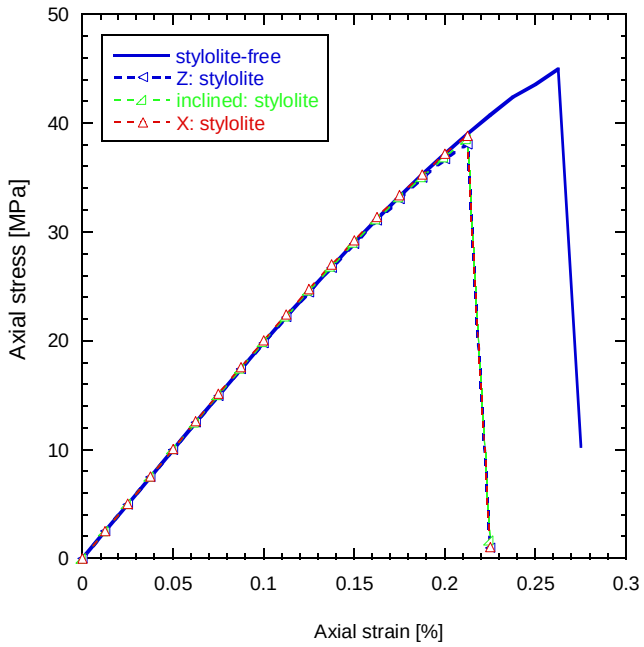
stylolite-free
Z: stylolite
inclined: stylolite
X: stylolite
Axial stress [MPa]
Axial strain [%]
0
10
20
30
40
50
0
0.05
0.1
0.15
0.2
0.25
0.3

Figure 15

B)

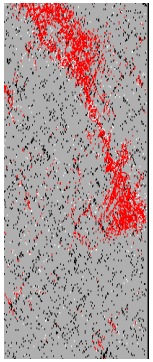

C)

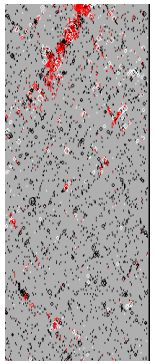

D)

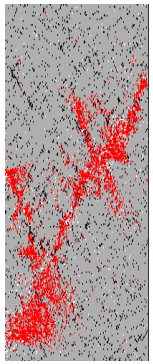

Figure 15

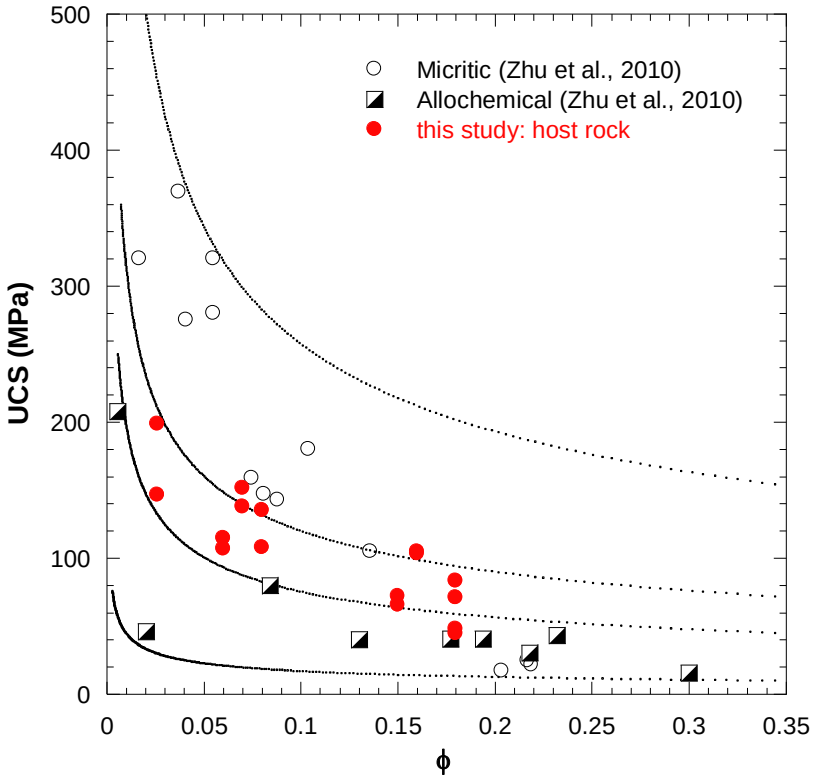
Micritic (Zhu et al., 2010)
Allochemical (Zhu et al., 2010)
this study: host rock
UCS (MPa)
ϕ
500
400
300
200
100
0
0
0.05
0.1
0.15
0.2
0.25
0.3
0.35

Figure 16

A)

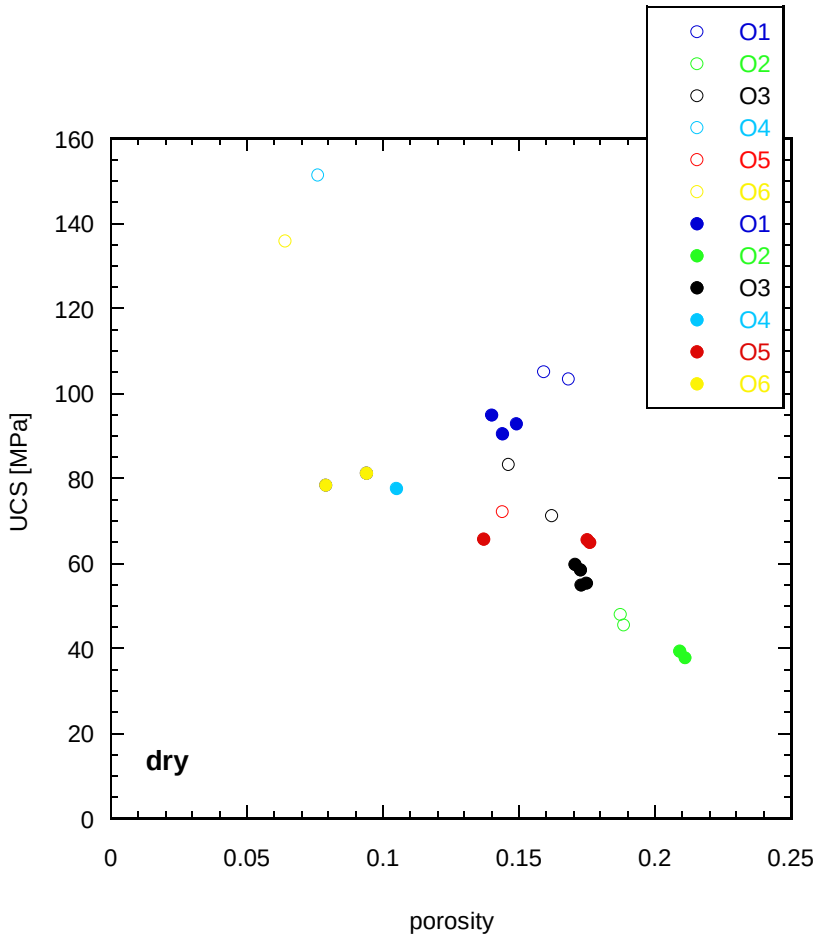
O1
O2
O3
O4
O5
O6
O1
O2
O3
O4
O5
O6
UCS [MPa]
porosity
dry
0
20
40
60
80
100
120
140
160
0
0.05
0.1
0.15
0.2
0.25

B)

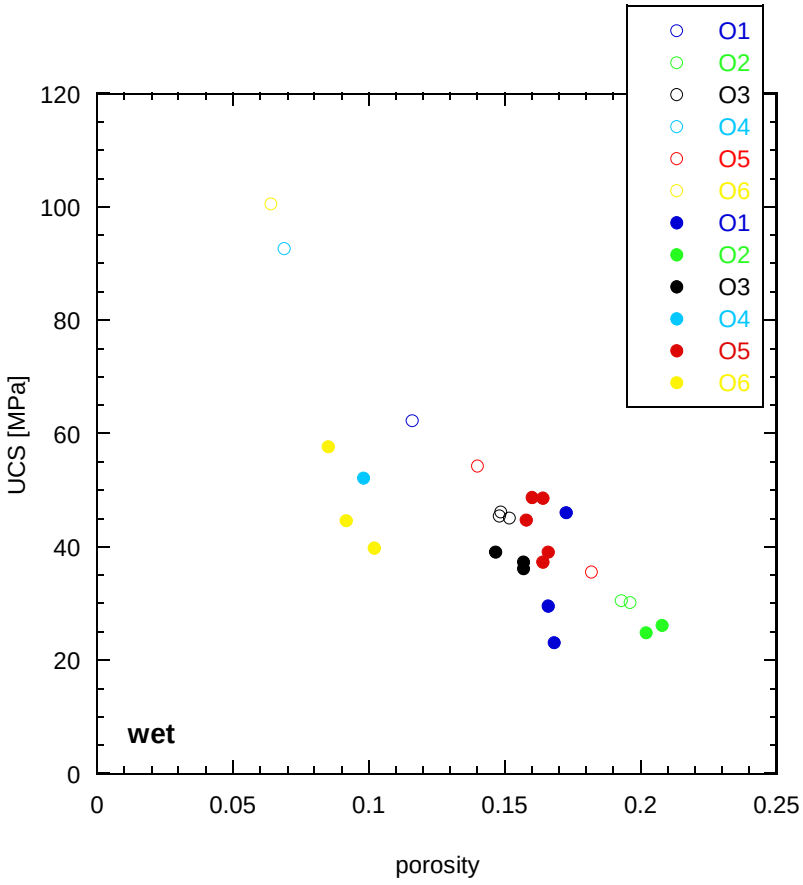
O1
O2
O3
O4
O5
O6
O1
O2
O3
O4
O5
O6
UCS [MPa]
porosity
wet
0
20
40
60
80
100
120
0
0.05
0.1
0.15
0.2
0.25

Figure 17

A)

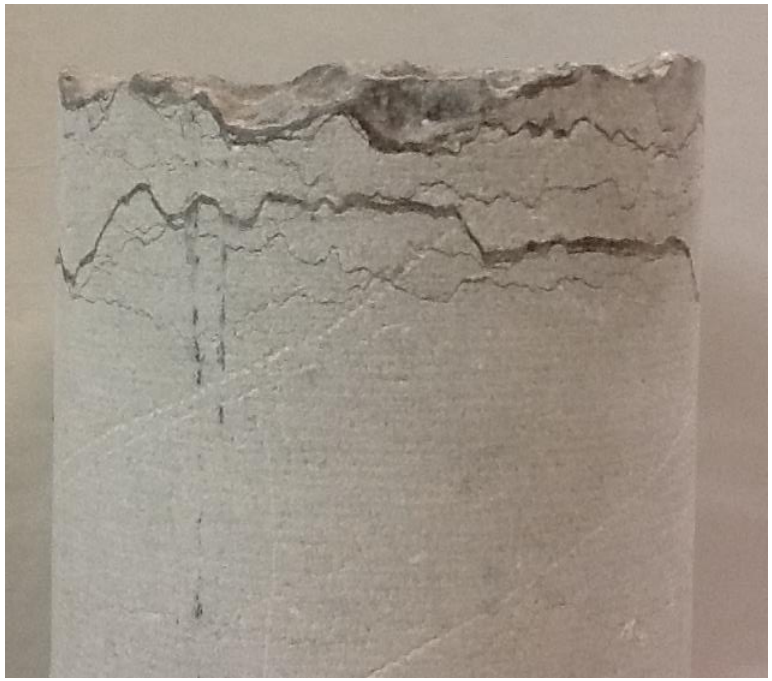

B)

C)

Figure 18